

NUCLEAR DATA AND MEASUREMENTS SERIES

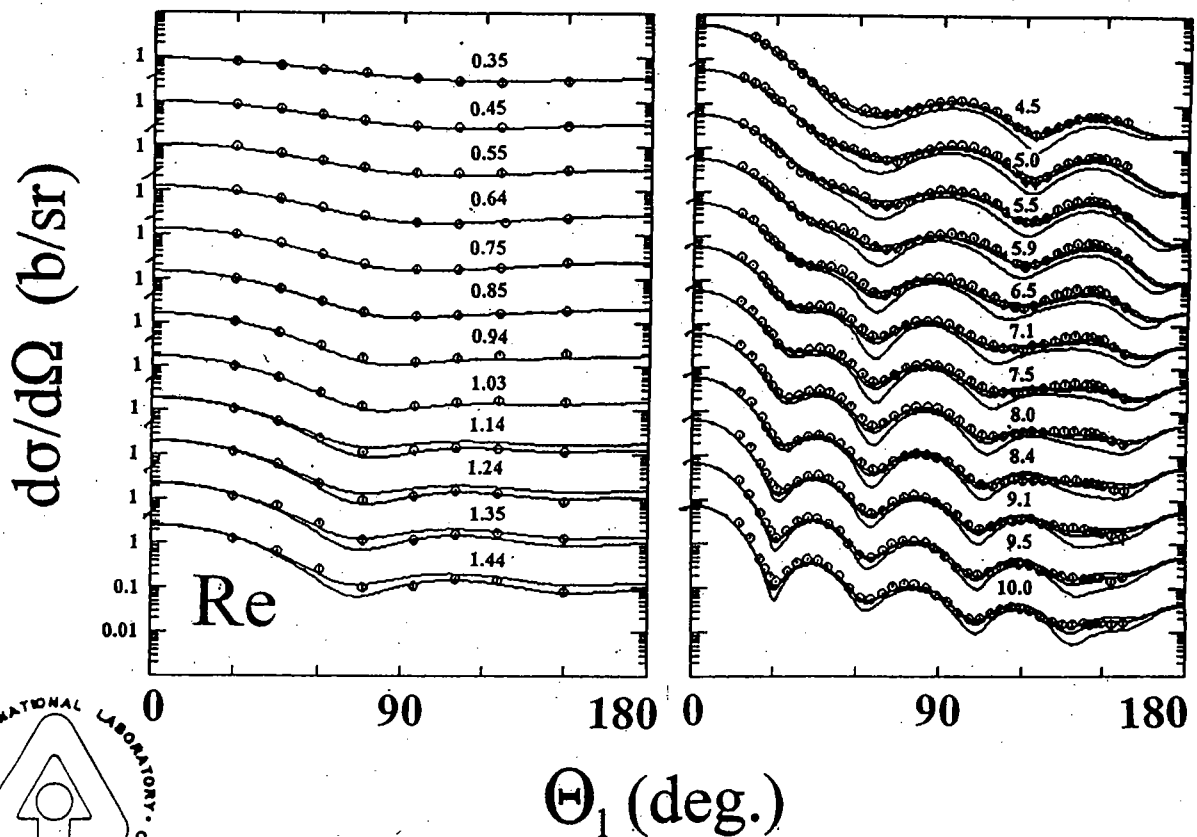
ANL/NDM-155

FAST-NEUTRON SCATTERING FROM ELEMENTAL RHENIUM*

by

Alan B. Smith

August 2003



ARGONNE NATIONAL LABORATORY, ARGONNE, ILLINOIS

Operated by THE UNIVERSITY OF CHICAGO

for the U. S. DEPARTMENT OF ENERGY

under Contract W-31-109-Eng-38

Nuclear Data and Measurement Series

Reports in the Argonne National Laboratory Nuclear Data and Measurement Series present results of studies in the field of microscopic nuclear data. The primary objective of the series is the dissemination of information in the comprehensive form required for nuclear technology applications. This series is devoted to: a) measured microscopic nuclear parameters, b) experimental techniques and facilities employed in measurements, c) the analysis, correlation and interpretation of nuclear data, and d) the compilation and evaluation of nuclear data.

Contributions to this Series are reviewed to assure technical competence and, unless otherwise stated, the contents can be formally referenced. This Series does not supplant formal journal publication, but it does provide the more extensive information required for technological applications (e.g., tabulated numerical data) in a timely manner.

Argonne National Laboratory, with facilities in the states of Illinois and Idaho, is owned by the United States Government, and operated by the University of Chicago under provisions of a contract with the Department of Energy.

Disclaimer

This report was prepared as an account of work sponsored by an agency of the United States Government. Neither the United States Government, nor the University of Chicago, nor any agency thereof, nor of their employees or officers, makes any warranty, expressed or implied, or assumes any legal liability or responsibility for the accuracy, completeness or usefulness of any information, apparatus, product, or process disclosed, or represents that its use would not infringe privately owned rights. Reference herein to any specific commercial product, process, or service by trade name, trademark, manufacturer, or otherwise, does not necessarily constitute or imply its endorsement, recommendation or favoring by the United States Government or any agency thereof. The views and opinions of the authors expressed herein do not necessarily state or reflect those of the United States Government or any agency thereof, Argonne National Laboratory, or the University of Chicago.

This report is available electronically at <<http://www.doe.gov/bridge>>. It is also available for a processing fee to the U. S. Department of Energy and its contractors in paper form from:-

U. S. Department of Energy

Office of Scientific and Technical information

P. O. Box 62

Oak Ridge, TN 37831-0062

Phone: (865) 576-8401

Fax: (865) 576-5728

E-mail: <reports@adonis.osti.gov>

Publications in the ANL/NDM Series

A listing of recent issues in this series is given below. Issues and/or titles prior to ANL/NDM-130 can be obtained from the National Technical Information Service, U. S. Department of Commerce, Technology Administration, Springfield, VA 22161, or by contacting the author of this report at the Nuclear Engineering Division, Argonne National Laboratory, 9700 South Cass Avenue, Argonne, IL 60439 (USA). In addition, the entire report series can be found on the Internet at the following URL: <<http://www.td.anl.gov/reports/ANLNDMReports.html>>, including abstracts, complete reports, and associated computer programs.

- A. B. Smith and P. T. Guenther
Fast-neutron interaction with the fission product ^{103}Rh
ANL/NDM-130, September 1993
- A. B. Smith and P. T. Guenther
Fast-neutron scattering from vibrational Palladium nuclei
ANL/NDM-131, October 1993
- A. B. Smith
Neutron interaction with doubly-magic ^{40}Ca
ANL/NDM-132, November 1993
- A. B. Smith
Fast-neutron scattering at $Z=50$:- Tin
ANL/NDM-133, September 1994
- A. B. Smith, S. Chiba and J. W. Meadows
An evaluated neutronic data file for elemental Zirconium
ANL/NDM-134, September 1994
- A. B. Smith and S. Chiba
Neutron scattering from Uranium and Thorium
ANL/NDM-135, February 1995
- A. B. Smith
Neutron scattering and models:- Iron
ANL/NDM-136, August 1995
- A. B. Smith
Neutron scattering and models:- Silver
ANL/NDM-137, July 1996
- A. B. Smith and D. Schmidt
Neutron scattering and models:- Chromium
ANL/NDM-138 June 1996
- W. P. Poenitz and S. E. Aumeier
The simultaneous evaluation of the standards and other cross sections of importance for technology
ANL/NDM-139, September 1997

- D. L. Smith and J. T. Daly
 A compilation of information on the $^{31}\text{P}(p,\gamma)^{32}\text{S}$ reaction and properties of excited levels in ^{32}S
 ANL/NDM-140, November 2000
- A. B. Smith
 Neutron scattering and models:- Titanium
 ANL/NDM-141, July 1997
- A. B. Smith
 Neutron scattering and models:- Molybdenum
 ANL/NDM-142, July 1999
- R. E. Miller and D. L. Smith
 Compilation of information on the $^{31}\text{P}(p,\gamma)^{33}\text{Cl}$ reaction and properties of excited levels in ^{33}Cl
 ANL/NDM-143, July 1997
- R. E. Miller and D. L. Smith
 A compilation of information on the $^{31}\text{P}(p,\gamma)^{28}\text{Si}$ reaction and properties of the excited levels in ^{28}Si
 ANL/NDM-144, November 1997
- R. D. Lawson and A. B. Smith
 ABAREX, a neutron spherical optical-statistical model code:- A user's manual
 ANL/NDM-145, June 1999
- R. T. Klann and W. P. Poenitz
 Non-destructive assay of EBR-II blanket elements using resonance transmission analysis
 ANL/NDM-146, 1998
- A. B. Smith
 ELEMENTAL-ABAREX:- A user's manual
 ANL/NDM-147, June 1999
- D. G. Naberejnev and D. L. Smith
 A method to construct covariance files in ENDF/B formats for critical safety applications
 ANL/NDM-148, June 1999
- A. B. Smith
 Neutrons and antimony:- physical measurements and interpretations
 ANL/NDM-149, July 2000
- A. B. Smith and A. Fessler
 Neutrons and antimony:- neutronic evaluations of ^{121}Sb and ^{123}Sb
 ANL/NDM-150, July 2000
- A. B. Smith
 Fast neutrons incident on Holmium
 ANL/NDM-151, December 2000
- R. D. Lawson and A. B. Smith
 Technical note:- Dispersion contributions to neutron reactions
 ANL/NDM-152, August 2001

A. B. Smith

Fast-neutrons incident on Hafnium

ANL/NDM-153, June 2001

D. L. Smith, Dimitri G. Naberejnev and L. A. Van Wormer

An approach for dealing with large errors

ANL/NDM-154, September 2001

ANL/NDM-155

FAST-NEUTRON SCATTERING FROM ELEMENTARY RHENIUM*

by

Alan B. Smith

Argonne National Laboratory, Argonne, Illinois; and
The Physicist's Consultative, Ottawa, Illinois

August 2003

Keywords:-

Measured neutron scattering, 0.3-1.5 MeV and 4.5-10 Mev. Optical-statistical and coupled-channels model analysis of experimental results. Basic and applied physical comments.

*This work supported by the United States Department of Energy under contract W-31-109-ENG-38.

TABLE OF CONTENTS

Abstract	7
I. Introduction	7
II. Experimental Procedures and Results	8
III. Physical Models	
III-A. Optical-Statistical Model (SOM)	9
III-B. Spherical Scalar and Vector Potentials (SOMV)	11
III-C. Coupled-Channels Rotational Models (ROTM)	12
III-D. Dispersive Effects	14
IV. Basic and Applied Comments	15
V. Some Comparisons with Other Potentials and Evaluated Files	
V-A. Comparisons with Other Potentials	18
V-B. Comparisons with Some Evaluated Files	20
VI. Concluding Remark	21
Acknowledgments	22
References	22
Appendices	
1. Prior Neutron Total Cross Section Data	24
2. Prior Neutron Elastic-Scattering Data	24
3. Prior Neutron Inelastic-Scattering Data	25
Tables	26
Figures	34

FAST-NEUTRON SCATTERING FROM ELEMENTAL RHENIUM

ABSTRACT

Results of measurements of neutron scattering from elemental rhenium over the incident-energy regions 0.3-1.5 MeV, and 4.5-10.0 MeV are presented. The first of these supplements previously-reported work at this Laboratory, and the second consists of information in a new energy range. These experimental results are interpreted in terms of optical-statistical and coupled-channels models, including consideration of dispersive effects, and of scalar and vector potentials. Some basic and applied physical implications of these considerations are discussed. Comparisons are made with other regional and/or global models, and with evaluated nuclear-data files used in applications.

I. INTRODUCTION

Elemental rhenium consist of a pair of isotopes:- ^{185}Re (37.4%) and ^{187}Re (62.6%). Both are highly deformed collective rotors with the low-lying structure of each built upon the $K=5/2^+$ band ($5/2^+$ [402]) with the particle configuration $(7/2^+)^2 (5/2^+)(9/2^-)^2$ arising from the $d^{5/2}$ shell [(MN59); (Pre62)]. Ground states are $5/2^+$ for both isotopes. The first excited states are $7/2^+$ and at approximately 130 keV, followed by $9/2^+$ levels at an excitation of approximately 300 keV (NNDC). The next well-deformed rotational band is a $K=9/2^-$ ($9/2^-$ [514]) configuration. In ^{185}Re the $9/2^-$ head of the latter band is at an excitation of approximately 370 keV, and in ^{187}Re at approximately 210 keV. With these collective structures one would expect relatively strong rotational effects in fast-neutron elastic- and inelastic-scattering processes. The only thing that is experimentally known of fast-neutron scattering from rhenium is the result of work at this Laboratory; some very early results at lower energies and the present lower-energy and 4.5 - 10 MeV results. The experimental knowledge of rhenium neutron total cross sections is little better, as summarized in **Appendix A-1**. At low energies neutron capture information is available (MY87) but it has minor influence on fast-neutron scattering. The lack of experimental neutron-scattering information for masses in this region of collective deformation is, unfortunately, quite typical.

Rhenium is not generally a concern in conventional fission-reactor fuel-cycle considerations. However, the metal is a high-temperature corrosion-resistant material for special uses; for example, in high-temperature nuclear space-power sources. Moreover, it is desirable to improve the understanding of the neutron interaction with nuclei in this mass region is a matter of wide practical concern. It was for these purposes that the present work was undertaken.

II. EXPERIMENTAL PROCEDURES AND RESULTS

Rhenium elastic- and inelastic-scattering cross sections at incident energies of less than 1.5 MeV were reported by the author and co-workers some time ago (SGW68). Since that report, a number of additional differential elastic- and inelastic-scattering measurements have been made over the same lower-energy range. All of these measurements employed the time of flight technique (CL55) with eight flight paths of about two meters length. Eight to ten measurements were distributed over the angular range of 25° - 160° at each incident energy. The neutron source was the ${}^7\text{Li}(p,n){}^7\text{Be}$ reaction (Dro87) below neutron energies of 1.5 MeV. This reaction emits a second neutron group that distorts inelastic-scattering results at excitations of approximately 450 - 500 keV. Below incident energies of 1.5 MeV the scattered-neutron resolutions were 25 - 50 keV, sufficient to resolve a great deal of the structure in the inelastic-scattering results. In total, approximately 118 scattered-neutron elastic and inelastic angular distributions were measured at incident energies of less than 1.5 MeV, about half of which have been published in the earlier work. All of these lower-energy measurements were made relative to carbon or zirconium total neutron scattering as reported in ref. (Lan+61). The lower-energy elastic-scattering results were energy-averaged and collapsed into twelve distributions in order to smooth fluctuations and reduce the statistical uncertainties. The resulting averaged distributions are illustrated in the left panel of Fig. II-1. The corresponding lower-energy inelastic-scattering results are discussed in Sec. III-C, below.

The second portion of the neutron-scattering measurements covered the neutron energy range 4.5 - 10 MeV with twelve approximately equal-energy-spaced distributions. Each of these higher-energy measurements involved ≈ 40 differential values distributed between $\approx 18^\circ$ and 160° . The ${}^2\text{D}(d,n){}^3\text{He}$ reaction (Dro87) was used as a neutron source at incident energies of 4.5 MeV and above. The scattered-neutron resolutions were ≈ 300 keV. Therefore, the inelastic scattering resulting from the excitation of low-lying levels of the rhenium isotopes was not clearly resolved. These higher-energy measurements involved the concurrent use of ten flight paths, each ≈ 5 meters in length. Cross sections were measured relative to the H(n,n) scattering standard (CSL83). The higher-energy "elastic"-scattering results are illustrated in the right panel of Fig. II-1.

All of the measurements used cylindrical samples of high-purity elemental metallic rhenium, approximately 2.0 cm in diameter and 2.0 cm long. All of the experimental results were corrected for angular-resolution, beam attenuation and multiple-event effects using monte-carlo procedures (Smi90).

Various versions of the time-of-flight system used in the above measurements operated at The Argonne National Laboratory for over thirty years. They are well described elsewhere (Smi92).

III. PHYSICAL MODELS

III-A. OPTICAL-STATISTICAL MODEL (SOM)

The weak-coupling optical-statistical model (SOM) [(Wol51); (Fes58)] was assumed as the starting point for the physical modeling. It is an energy-average model, reflecting gradual energy-dependent trends of the experimental observables, but not the detailed underlying resonance structure. Above a few keV the microscopic resonances underlying the observed phenomena grossly overlap to form smooth energy-dependent averages consistent with the SOM concepts, therefore the present considerations started at 50 keV and extended upward in energy to approximately 10 - 12 MeV where they were terminated due to the lack of experimental information at higher energies. Throughout this work the real potential was assumed to have the Saxon-Woods form, the imaginary potential the Saxon-Woods-Derivative form, and the spin-orbit potential the Thomas form (Hod63). Both direct and compound-nucleus interactions were given detailed attention. Eighteen ^{185}Re and eighteen ^{187}Re excited states were explicitly considered up to excitation energies of ≈ 1.0 MeV. The respective excitation energies, spins and parities were taken from the Nuclear Data Sheets (NNDC). Higher-energy excitations were considered in the context of statistical evaporation processes as set-forth by Gilbert and Cameron (GC65). The calculations included resonance width-fluctuation and correlation corrections following the methods of Moldauer (Mol80). Compound-nucleus processes were considered only as relevant to neutron total and scattering processes. Multiple-neutron and charged-particle emission is not significant at the energies of the present work. All of the SOM calculations were carried out using the code ELEMENTAL ABAREX (Smi99), which concurrently treats each of the two isotopes of elemental rhenium. In doing so real and imaginary iso-vector potentials can be examined, assuming the same geometries as those of the scalar potentials. The spin-orbit potentials were fixed to the real values of ref. (WG86).

The SOM parameters were determined by explicitly chi-square fitting the neutron total and differential scattering cross sections. The model fitting proceeded through six sequential steps. i) Six parameter fitting varying real and imaginary potential parameters from which the real-potential diffuseness, a_v , was fixed and the fitting proceeded to the next step. ii) Five parameter fits from which the real-potential reduced radius, r_v where $R_v = r_v A^{1/3}$, was determined and fixed for the subsequent steps. iii) Four parameter fitting from which the reduced imaginary-potential radius, r_w , was determined and fixed. iv) Three parameter fits from which the imaginary diffuseness, a_w , was determined and fixed. v) Two parameter fitting giving the real potential strengths, V . And finally, step vi) one parameter fitting from which the imaginary strength, W , was determined. The entire procedure was repeated several times in an iterative manner, using the results of the prior fitting cycle as the starting point for the current one. The data base for the fitting included all of the differential-scattering data of Fig. II-1. The uncertainties of the scattering data were taken as indicated by the measurements, except for the low-energy averaged data where 5% was subjectively chosen. The total cross sections (Appendix A-1) at the energies of the scattering measurements were concurrently included in the fitting procedures. In doing so the total-cross-section data were averaged over approximately

100 keV and given a weight that was equivalent to that of four or five differential-scattering values. The experimental resolutions used in the scattering measurements below ≈ 1.5 MeV were such as to resolve the elastic from all inelastic-scattering components. However, for the higher-energy data (4.5 - 10 MeV) the observed scattering distributions included the contributions due to the excitation of the first two or three excited levels of each isotope with the elastic component. The fitting was adjusted so as to include these inelastic contributions with the elastic scattering, reflecting the experimental resolutions above 4.5 MeV.

The above fitting procedures led to the SOM parameters given in **Table III-A-1** (Throughout this work potential parameters are given to sufficient precision to make possible accurate reproduction of calculated results. These precisions do not necessarily imply uncertainties.) The SOM parameters may reflect the inappropriateness of the model for describing the fast-neutron interaction with these two highly collective rotational isotopes. There are several causes for concern. The real-potential strength is essentially constant, not decreasing with energy as one would expect from the non-locality of the nuclear force (PB62), and as encountered in commonly used "global" and "regional" models [(KD03); (Hod94)]. The real reduced radius is rather small. This tends to be characteristic of SOM representations of the neutron interaction with highly collective targets in this mass region [(Smi00); (Smi01)]. The imaginary-potential strength has two branches reflecting a sharp energy dependence. The imaginary radius is unusually large. The imaginary diffuseness is quite small at low energies and rapidly increases with energy. These SOM parameters are based upon the interpretation of the present experimental work which only extends to ten MeV. Extrapolation to higher energy, as discussed below in the context of dispersion effects, may be valid to some extent. Despite the difficulties, the SOM may be of practical use in some applications. It gives a very good representation of the neutron total cross section of elemental rhenium from a few keV to more than 15 MeV, as illustrated in **Fig. III-A-1**. The calculated results are within several percent of the measured values. Deviations between measurement and calculation are less than variations within the experimental data alone. Furthermore, the experimental-total-cross-section data sets somewhat vary in magnitude and the energy-dependent shape is not entirely consistent with any optical-model. The SOM does not do well in describing the measured "elastic"-scattering distributions, as illustrated in **Fig. III-A-2**. The agreement between measurement and calculation is reasonably good up to incident energies of 1.5 MeV. In this low-energy region the compound-elastic contribution is strongly influenced by competition with compound-nucleus inelastic processes which were given detailed attention in the calculations. Above ≈ 1.5 MeV the measured "elastic" distributions also include growing contributions from inelastic scattering which increasingly is dominated by direct-reaction processes involving the collective rotational properties of the two rhenium isotopes. Such direct-reaction processes are beyond the scope of the SOM, and are dealt with below in the context of rotational coupled-channels models. The consequence is a distortion of the SOM scattering calculations in the few-MeV region, particularly in the minima of the measured distributions which contain significant inelastic direct-reaction contributions.

III-B. SPHERICAL SCALAR AND VECTOR POTENTIALS (SOMV)

From basic concepts of nuclear forces and supported by some experimental evidence [(GPT68); (Sat69); (Hod94) and (BG69)] the real and imaginary SOM potentials are frequently expressed in the forms

$$\begin{aligned} V &= V_0 \mp V_1 \cdot \eta \\ \text{and} \\ W &= W_0 \mp W_1 \cdot \eta, \end{aligned} \tag{III-B-1}$$

where V_0 (W_0) is the “scalar” term and V_1 (W_1) is the “vector” term, η is the nuclear asymmetry equal to $(N-Z)/A$, and the signs are negative for neutron induced processes and positive for proton processes. These expressions are manifestation of the iso-spin dependence of the potential that is discussed in Sec. IV, below. They are frequently used in practical data interpretations, as in this case. Herein the SOM with the formulations of Eqs. III-B-1 is termed the SOMV. Various values of V_1 are found in the literature, generally in the range 15 - 30 MeV, with 16 and 24 MeV commonly used values [(MY87); (Smi00)]. The imaginary “vector” values are generally taken to be half those of the real potential. The two isotopes of rhenium were dealt with in detail in the above SOM derivation, including size, compound-nucleus structure and natural abundance. However, the asymmetry and its implications on the potentials were not considered. The asymmetries of ^{185}Re and ^{187}Re differ by less than 4%. Therefore, the impact of the “vector” term of Eq. III-B-1 is small; e.g., for a typical V_1 value of 16 MeV the real potentials of the two isotopes will differ by approximately 0.7 MeV, a value which is less than 1.5% of the entire real potential and thus hard to detect from experimental interpretations. The impact of W_1 is even smaller.

All the fitting procedures used to determine the SOM were explicitly repeated to obtain the SOMV, including selection of geometric factors. Two choices of V_1/W_1 were used; 16/8 MeV and 24/12 MeV. The resulting potential parameters are given in Tables III-B-1 and III-B-2, respectively. The Table III-B-1 SOMV potential gives a description of the observed rhenium total cross sections very similar to that obtained with the SOM over the energy range of the present interpretations, as illustrated by comparing Fig. III-B-1 and Fig. III-A-1. Above 10 MeV the SOMV total cross section calculations tend to be several percent smaller than the results of the SOM calculations, and smaller than the measured values. This is the region of energy extrapolation of both the SOM and SOMV potentials as described in Sec. III-D. The discrepancy vanishes with alternate choices for extrapolation in energy. Fig. III-B-2 compares the measured differential “elastic”-scattering results with the those of the SOMV calculation using the potential of Table III-B-1. The results are essentially identical to those obtained with the SOM. The “vector” potential of the above SOMV was increased to V_1/W_1 equal 24/12 MeV in order to examine the effect of alternate “vector” potential choices. 24 and 12 MeV are commonly used values found in the literature (Smi99A). The entire fitting procedure of the SOMV was repeated, resulting in the potential parameters of Table III-B-2. The calculated and measured total cross sections and differential “elastic” scattering cross sections were compared,

with results that are essentially identical to those illustrated in **Fig III-B-1** and **Fig. III-B-2**. Generally, it was concluded that the various SOMV potentials lead to no improvement over the simple SOM potential in the present application. Any differences probably reflect reasonable statistical fluctuations in the respective fitting procedures. This is not surprising as for the two rhenium isotopes the vector potential effects are very small, generally below the experimental sensitivity.

III-C. COUPLED-CHANNELS ROTATIONAL MODELS (ROTM)

The various versions of the SOM fall qualitatively short of reasonably describing the scattering of fast neutrons from these two highly collective rotational isotopes. In particular, they do not describe the elastic or inelastic scattering by large amounts. One should expect the scattering between the $5/2^+$ (g.s.), $7/2^+$ ($E_x \approx 130$ keV), and $9/2^+$ ($E_x \approx 300$ keV) levels of the ground-state $K=5/2^+$ band to be strongly coupled. In the ROTM interpretation these first three yrast states of the $5/2^+$ g.s. rotational band of each of the two isotopes were coupled together. The ^{185}Re deformations were taken to be $\beta_2 = 0.22$ and $\beta_4 = -0.085$ and those of ^{187}Re to be $\beta_2 = 0.21$ and $\beta_4 = -0.085$, as indicated by systematics and as cited in the literature [(GPA72); (MY87)]. With these choices a comprehensive rotational fitting procedure was carried out using the geometric form factors of the above SOM and a similar fitting rational. All of the calculations employed the coupled-channels method (Tam65) implemented with the coupled-channels code ECIS (Ray96). The latest version of that code will handle compound-nucleus processes in the same way as the ABAREX used in the SOM fitting. Each step of the fitting consisted of a ^{185}Re and a ^{187}Re calculation, assuming that the experimental data applied only to the respective isotope. The resulting two parameters sought in that particular step of the fitting were then averaged, weighting with the isotopic abundance, to obtain the "elemental" value. The procedure clearly does not consider vector potential effects but those have been shown to be negligible in the present application. All the fitting was done with the differential scattering measurements. The total cross sections were considered only in comparisons with the calculated results after the fitting.

The ROTM elemental parameters following from the above fitting procedure are given in **Table III-C-1**. These parameters lead to the elemental neutron total cross sections compared with the available experimental information in **Fig. III-C-1**. The quality of the description of the experimental results approaches that of the SOM even though no total cross sections were involved in the fitting, as in the SOM case. This suggests that the measured total and differential-scattering cross sections are reasonably consistent. **Fig. III-C-2** compares the experimental scattering data with the results of calculations using the ROTM. The experimental observables are well described by the model. In particular, the large discrepancies so evident with variants of the SOM are not present. This is clearly a reflection of the rotational nature of the model in this application. Below incident energies of 1.5 MeV the single elastic distributions are reasonably consistent with the measured values as one would expect from the estimated experimental energy resolution. At and above 4.5 MeV the calculations combining

the elastic contribution with those from the first two inelastic groups of the g.s. rotational band are clearly most consistent with the data, as expected from the estimated energy resolution of the measurements.

The above elemental ROTM results are quite consistent with those obtained if one treats ^{185}Re and ^{187}Re individually and assumes that the experimental elemental data is explicitly applicable to either of the isotopes. With these assumptions the above isotopic fitting procedures were repeated individually for each of the two isotopes to obtain "isotopic" potential parameter sets. These are illustrated for ^{187}Re in **Table III-C-2**. The isotopic potential parameters are very similar to those of the ROTM, as are comparisons with the measured values. This again suggests that "vector" potential effects are not a serious consideration in the present application, and that the differences due to compound-nucleus properties and size effects are small.

The present inelastic-scattering results were combined with the early work of ref. (SGW68). The combined set was ordered by incident and excitation energy, and then averaged over approximately 50 keV incident-energy bins. Uncertainties were assigned to the averaged values as estimated by the author. These inelastic-scattering excitation functions are correlated with the known excited levels in the isotopes ^{185}Re and ^{187}Re in **Table III-C-3**. The first four inelastically-scattered neutron groups seem quite clearly associated with well-defined levels in the two rhenium isotopes. The fifth observed inelastic-neutron group is in the energy region which is distorted by the second neutron group of the source reaction, as noted above. It doubtless consists of contributions from three reported levels in the two isotopes, but also includes a large contribution from elastic-scattering of the second source-reaction group. This conclusion is strongly supported by the cross section magnitudes, as discussed below. The sixth inelastic group of **Table III-C-3** may be associated with at least six reported levels in the two isotopes. Four additional inelastic-neutron "groups" were observed but, in the context of the rapidly increasing level densities of each of the two isotopes and deteriorating experimental energy resolution, correlation between observation and level structure rapidly deteriorates above excitations of 0.6-0.7 keV, and no attempt was made to establish such associations. The cross sections for the above excitations were calculated with the ROTM potential with the results shown in **Fig. III-C-3**. The agreement between measured and calculated results for levels 2, 3, 4 and 6 is reasonably good given the uncertainties in the measured and calculated values. The measurements relative to level 5 are grossly larger than predicted by the model. This is the level greatly distorted by the elastic scattering of the second group from the source reaction. The calculated values for the excitation of the first (1) level are significantly larger than the measured quantities over much of the experimental energy range. There can be little doubt that the observed cross sections are due to excitation of the yrast ($7/2+$) levels in each of the rhenium isotopes. Furthermore, much of the cross section consists of the direct-reaction component which is strongly influenced by the magnitude of β_2 . The comparisons of **Fig. III-C-3** suggest that the β_2 used in the above ROTM calculations is too large. The entire ROTM fitting, outlined above, was repeated with smaller values of β_2 . After several attempts it was concluded that the inelastic excitation of the first level was best calculated when the β_2 of each isotope was reduced

by approximately 15% from the values used in the above ROTM calculations. The potential parameters following from the fitting with these smaller values are essentially identical to those of the ROTM. The resulting calculated inelastic excitation of the first level was in much improved agreement with experiment, as illustrated in **Fig. III-C-4**, and the description of the differential-scattering distributions was essentially the same as achieved with the ROTM potential, shown in **Fig. III-C-2**. The evidence is not unequivocal, but the inelastic-scattering measurements suggest that the β_2 used in the ROTM model, and as reported in the literature, is too large. More precise inelastic-scattering evidence may well support this conclusion.

III-D. DISPERSION EFFECTS

It is well known that there is a dispersion relationship coupling real and imaginary potentials and reflecting causality [(Sat83); (Lip66); (Pas67) and (Fes58)]. This relationship is frequently expressed in the form

$$J(E)_V = J(E)_{HF} + (P/\pi) \cdot \int [J_w(E')/(E - E')] \cdot dE' \quad \text{III-D-1}$$

where J_V is the strength of the real potential, J_{HF} that of the local-equivalent Hartree-Fock potential, and J_w the strength of the imaginary potential. "P" is the principle value of the integral which is evaluated from $-\infty$ to $+\infty$. Here, and throughout this section, strengths are given in the form of volume-integrals-per-nucleon unless otherwise stated. The above integral can be broken into surface, ΔJ_{sur} , and volume, ΔJ_{vol} components

$$\Delta J_{sur} = (P/\pi) \cdot \int [J_{sur}(E')/(E - E')] \cdot dE' \quad \text{III-D-2}$$

and

$$\Delta J_{vol} = (P/\pi) \cdot \int [J_{vol}(E')/(E - E')] \cdot dE'. \quad \text{III-D-3}$$

Then $J_{vol}(E) = J_{eff}(E) + \Delta J_{sur}(E)$ and $J_{eff}(E) = J_{HF}(E) + \Delta J_{vol}(E)$, where $J_{sur}(E)$ and $J_{vol}(E)$ are surface- and volume-imaginary potential strengths, respectively. J_{HF} and ΔJ_{vol} are both approximately linear functions of energy in the range of the present considerations, thus the individual components can not be experimentally resolved. The effect of **Eq. III-D-2** is to add a surface component to the real potential that is some fraction of the imaginary potential. The magnitude of this contribution was calculated using the methods of Lawson (LGS87) and Lawson and Smith (LS01). The latter reference presents a detailed description of the theory and method, and includes a FORTRAN code for executing the calculations. In the present application it was assumed that ΔJ_{sur} retained the geometric parameters and Saxon-Woods-Derivative form of the imaginary potential, varying only in magnitude. This is an assumption that is not necessarily true, but there appears to be no guidance as to alternate shapes. The experimental data base and associated models are strictly relevant to only the energy range of 10 MeV or less. It was assumed that the surface-imaginary potential was entirely a surface effect

up to 10 MeV, and then fell linearly to zero at 80 MeV. Concurrently, the volume-imaginary potential was taken to rise from zero at 10 MeV to 80 MeV where it took the J_{sur} 10 MeV magnitude, and then remained constant to infinity (this energy extrapolation was used in the above considerations). Further, the imaginary potential was assumed to be zero at the Fermi Energy (E_F) and to have a quadratic energy dependence from E_F to zero energy. The Fermi energy was taken to be -7.0 MeV as determined from the mass tables (TUL90). Throughout, the considerations, the entire imaginary potential was taken to be symmetric about the Fermi energy.

Following the above-outlined procedures and the methods of ref. (LS01), the above ΔJ_{sur} value was calculated from the SOM. These calculations assumed the higher-energy branch of J_w of **Table III-A-1** as being more representative of the SOM and less distorted by deformation effects. The calculations provide the contribution of the imaginary potential that must be reflected into the real potential due to dispersive effects. The energy dependence of the fraction of J_w that is reflected into the real potential is illustrated in **Fig. III-D-1**. It decreases from near unity at zero energy to modest negative values at 20 MeV. These magnitudes and energy dependancies are somewhat dependent on the energy extrapolations cited above. This dispersive fraction was converted to a potential fraction assuming the potential geometries of the SOM potential (**Table A-III-1**).

Using the above "DISP" contribution the entire fitting of the SOM potential was repeated. The resulting model parameters are given in **Table D-III-1**. They are similar to those of the simple SOM (**Table III-A-1**). There are some changes in the real-potential geometry and the real-potential strength is noticeably reduced, as one would expect from the introduction of a surface real potential. The corresponding calculated elemental rhenium total cross sections are in good agreement with measured values below 10-12 MeV, as illustrated in **Fig. III-D-2**, but then fall a bit low, suggesting that the higher-energy portions of the potential employed in calculating the dispersive contribution of **Fig. III-D-1** is not quite correct. The dispersive calculations result in the differential distributions that are essentially identical to those obtained with the SOM. The above SOM dispersive exercise was repeated using the ROTM, and resulted in the potential parameters of **Table III-D-2**. These values are consistent with those of the simple ROTM model given in **Table III-C-1**. They result in a reasonable description of the elemental rhenium total cross sections, as illustrated in **Fig. III-D-3**. The same is true for the calculated differential "elastic" scattering from elemental rhenium as illustrated in **Fig. III-D-4**. Though dispersive effects may well be a physical reality, they do not have significant effects in the present studies.

IV. BASIC AND APPLIED COMMENTS

The real radius of the SOM is small as observed in spherical models of the neutron interaction with the neighboring rotational elements Ho and Hf [(Smi00) and (Smi01)]. Concurrently, unusual SOM energy-dependent imaginary-potential strengths and sizes are often encountered, as in this rhenium case. These are likely reflections of the inappropriateness of the

SOM in such applications. The rhenium ROTM real-potential geometries are similar to those of elemental Ho and Hf [(Smi00); (Smi01)], to those reported for relevant regional models (You86) and to systematics. For example, the systematics of ref.(Smi98) predict a $Re a_v$ within 7% of that of the ROTM, and an r_v within 0.8% that of the ROTM. The r_v of ref. (You87) differ from those of the ROTM by only 1.2%, and the a_v by only 4.2%. The present ROTM r_w is 2.6% larger than that of Ho and Hf, and the a_w 8.8% smaller. In these latter cases the imaginary parameters are not as well defined so one should expect larger differences. Generally, the geometries of the present ROTM seem consistent with comparable rotational models in this mass region.

The above experimental interpretations are limited to 10 MeV and less. At these energies it was assumed that the absorption was entirely a surface phenomena. This is generally consistent with regional and global trends, as illustrated in ref. (MY87) where the onset of volume absorption is set at 9 MeV. The dispersion considerations, discussed above, introduced a volume absorption at 10 MeV, slowly increasing with energy. It is used in the extrapolations of the potentials to higher energies and may not be quantitatively valid. A more serious concern at higher energies is probably the opening of additional neutron channels not considered in the present interpretations. In fact, neither the shapes or magnitudes of surface and volume absorptions are reasonably established at higher energies. Intuitively, one might expect that absorption slowly makes a transition from a surface phenomena to a volume effect with increasing energy, rather than attributing absorption to two independent components.

The isotopic-spin dependence of the optical model results in proton and neutron potential strengths that are related to iso-spin through the expression

$$J_i = J_{oi}(1 \mp \xi_i \cdot \eta) \quad \text{IV-1}$$

where J_i are potential strengths expressed as volume-integrals-per-nucleon, η is the nuclear asymmetry $(N-Z)/A$, “i” may be either V or W for the real or imaginary potentials respectively, the sign is “+” for proton processes and “-” for neutron processes, and ξ_i is a constant (Lan62). The “scalar” and “vector” potentials employed in the fitting of Sec. III-B are the frequently used manifestations of Eq. IV-1. Neutron scattering studies lead to ξ_v values near unity [(FCR77); (HW72); (Smi98)]. However, those ξ_v values are nearly twice those suggested from nucleon-nucleon scattering and (p,n) studies. More accurately, Eq. IV-1 should be (Chi+90)

$$J_v = (r_v)^3 \cdot K_{0v} (1 \mp \xi_v \cdot \eta) \quad \text{IV-2}$$

where K_{0v} is a constant and r_v has an appropriate mass dependence. Using an r_v mass-dependent expression such as (Smi98)

$$r_v = 1.1685 + 0.37225/A^{1/3} \quad \text{IV-3}$$

the neutron scattering data implies a ξ_v of approximately 0.5, similar to the values suggested

from nucleon-nucleon scattering and (p,n) studies [(Chi+90); (GMP70); (GPT68); (BFG69)]. **Eq. IV-1** is a reasonable starting point for comparing real-potential strengths over a limited mass range, but the results may be seriously influenced by shell and collective structural effects. In particular, coupling effects in interactions with highly collective nuclei, as in the present work, may very much distort the behavior predicted by **Eq. IV-1** (Com79). Recent work by the author has dealt with the fast-neutron interaction with three similar collective rotational targets; elemental Ho (¹⁶⁵Ho) (Smi00), elemental Hf (Smi01), and elemental Rh (the present work). The average elemental nuclear asymmetries of these three targets are very similar, respectively 0.186, 0.193 and 0.195. In each case the fast-neutron interaction was described in the context of a rotational model coupling the first three states of the g.s. rotational band. The real potential strengths for the three targets are; for Ho $J_v = 444.39 - 3.558 \cdot E$, for Hf $J_v = 455.98 - 2.587 \cdot E$, and for Re $J_v = 430.16 - 2.969 \cdot E$. These are very similar values with an average at $E = 0$ of $443.5 \pm 1.7\%$. At 10 MeV, the upper energy of the respective interpretations, the average is $413.13 \pm 2.1\%$. Of, course, if one constructs the J_{0i} of **Eq. IV-1** the result will be essentially a renormalisation of the three J_v values depending on the magnitude of ξ_v one assumes. Because of the similarities of the asymmetries and the J_v magnitudes, the measurements of the neutron interaction with these three targets do not support nor refute **Eq. IV-1** in the context of the real potential. The magnitudes of the imaginary strengths deduced from the measurements of the neutron interaction with the same three targets are; for Ho $J_w = 22.4 + 2.151 \cdot E$, for Hf $J_w = 19.5 + 2.419 \cdot E$, and for Re $J_w = 18.3 + 2.258 \cdot E$. Again, the three values are very similar, with a zero-energy average value of $20.0 \pm 6\%$, although there is a trend for the value to decrease with asymmetry as indicated by **Eq. IV-1**. As for the J_v values, they are consistent with **Eq. IV-1** but provide little further definition. **Eq. IV-1** relates the strengths of potentials in neutron and proton scattering. Unfortunately, the author could find no (p,p) scattering or (p,n) reaction data relevant to this work in the literature, and neither could information specialists at the NNDC.

Dispersive effects doubtless are a factor in the neutron interaction with the isotopes of rhenium. With some simplifying assumptions, they were included in the above spherical and rotational interpretations. Their presence did not notably improve the description of the observables. There were some changes in the potential parameters (e.g., compare **Tables III-C-1** and **III-D-2**), generally of a form that one would expect from the introduction of the dispersion effect (e.g., some decrease in r_v). However, from the practical point of view, there is little justification for the additional complexity of the dispersion calculations in this particular case.

Attention was given to vector potentials in both a spherical and deformed context. Any effect they might have had was very much masked by the unavoidable experimental uncertainties in the data being analyzed. This conclusion is not surprising in view of the very similar asymmetries of the two isotopes of rhenium.

The above rotational potentials have energy dependencies that define the effective mass, m^* , through the equation

$$(m^*/m) = 1 - (dV^L/dE) \quad \text{IV-3}$$

where m is the nucleon mass and V^L the local real potential. This ratio is 0.667 for the above ROTM potential given in **Table III-C-1**. It is shown in refs. [(BDS79); (MN81) and (Bau+82)] that nonlocality leads to the expression

$$(m^*/m) = 0.64 + 0.36[1.0 + \text{abs}(E - E_F)/(2\hbar W_0)]^2 \quad \text{IV-4}$$

where E_F is the Fermi energy and $\hbar W_0 = 41/A^{1/3}$. Well away from E_F **Eq. IV-4** leads to a (m^*/m) ratio of approximately 0.68 which is reasonably consistent with the nuclear matter estimate (GPT68) and remarkably close to the value given by the present ROTM potential. Concurrently, the zero end point of ROTM real potential is 148 MeV which approaches the value of the global analysis of ref. (Bau+82). The above m^* considerations apply to the other variants of the rotational coupled-channels model discussed in **Sec. III-C**. Clearly, the energy dependencies of the various SOM formulations are inconsistent with the above concepts.

The above discussion of inelastic scattering (**Sec. III-C**) and **Figs. III-C-3** and **III-C-4** suggest that the β_2 values for the two isotopes used in the primary ROTM calculations are 10-20% too large. Alternatively, more complex coupling schemes may be more appropriate, as in ref. (Com79). Unfortunately, the measured neutron inelastic-scattering data is not of sufficient quality or detail for a more quantitative examination of the degree of deformation. What is needed is a careful set of measurements of the cross sections for the inelastic excitation of the first few excited levels of both rhenium isotopes. Such measurements are feasible but demanding.

V. SOME COMPARISONS WITH OTHER MODELS AND EVALUATIONS

V-A. COMPARISONS WITH OTHER POTENTIALS

There are a number of collective models of the fast-neutron interaction with nuclei in this mass region reported in the literature. It is of interest to compare some of the corresponding potentials to that of the ROTM of the present work. In making these comparisons a rotational rhenium model with the deformations of the ROTM (**Table III-C-1**) was assumed. The corresponding strengths and geometries were taken as reported by the various authors. Nuclear asymmetry was considered when given. These comparisons were confined to the total cross sections at incident energies of < 20 MeV, and to differential "elastic" scattering at energies of 4.5 to 10 MeV. Lower-energy scattering was not considered as those distributions are "bland" and not particularly sensitive to choice of potential. Inelastic scattering was not considered as there remains the question of the magnitude of the deformations. These potential comparisons are intended to be illustrative and are confined to the following five potentials:-

- A. The reference point was taken to be the present ROTM potential (**Table III-C-1**).
- B. The potential for the neutron interaction with holmium by Smith (Smi00).

- C. The potential given by Macklin and Young (MY86) in a study of rhenium neutron capture.
- D. The potential for neutron total and scattering cross sections of hafnium (Smi01).
- E. A general potential for the fast-neutron interaction with holmium by P. Young (You86).

The fast-neutron total cross sections of elemental rhenium, as calculated with the above potentials (A-E) are compared with the available experimental information in **Fig. V-A-1**, Panel "A" of the figure references the ROTM of the present work. The calculated results are arguably lower than the measured values by a percent or two in some energy regions. As discussed in **Sec. III**, there are some questions about these small differences and the general energy dependence of the experimental values from which it is not clear that these small differences do not reflect experimental problems within the limited data base. Panel B of the figure references potential B. That potential is largely based upon an interpretation of neutron scattering from holmium over the energy range 4.5-10 MeV. Over that energy range it gives a very good description of the rhenium total cross sections. The calculated total cross section results are not quite as suitable at lower and higher energies but the differences between calculated and measured values are relatively small (less than 5-6%). Panel C compares measured total cross sections with those calculated with potential C. The agreement is very good, perhaps arguably better than obtained with the reference ROTM. The calculated total cross sections tend to be slightly larger than the measured values over most of the energy range. Panel D compares measured values with those calculated with potential D. The latter resulted from an interpretation of total and scattering cross sections of elemental hafnium, largely below 10 MeV. In the region of the primary scattering cross sections (4.5 - 10 MeV) the agreement is reasonably good, but at lower energies the calculations deviate from the measured rhenium values by large amounts. This reflects the physical reality that the measured hafnium and rhenium total cross sections are very different in this energy region. Panel E compares measured total cross sections with those calculated with potential E. Potential E is a regional representation and thus is not as specifically suitable as either the reference potential A or the specific rhenium potential C. These total-cross-section comparisons suggest, not surprisingly, that specific potentials based upon the rigorous interpretation of measured values are most suitable for total-cross-section prediction. Also, there are structural differences between nearby targets that can have a considerable effect on the corresponding potentials and their prediction of total cross sections. Unfortunately, in the case of rhenium experimental knowledge of neutron total cross sections is meager, and nonexistent above 15 MeV. Given the present experimental situation, the reference potential A (ROTM) or potential C give the best representations of rhenium total cross sections of the five potentials considered here.

The same type of comparisons are made between measured and calculated "elastic" scattering in **Fig. V-A-2**. The experimental reference is again the 4.5-10 MeV scattering data of the present work. There is no higher-energy experimental information and the lower-energy measured values lack the "character" for reasonable comparisons. The same A through E

potentials cited above are used, with "A" (ROTM) taken as the reference. It is evident from panel A of **Fig. V-A-2** that the ROTM of the present work gives an excellent description of the measured values as discussed in **Sec. III-C**. The calculated distributions combining elastic and first two inelastic groups are in nearly exact agreement with measured values which have a corresponding experimental resolution. The agreement for potential B, as shown in panel B of the figure, is also good. This is perhaps not surprising as potential B was largely deduced from differential scattering measurements in this energy range. Potential C does well in describing the total cross sections but it is not particularly suitable for describing the differential scattering (panel C). Potential D is an improvement, as illustrated in panel D. Like potentials A and B, its derivation was very much dependent on differential scattering in the 4.5 to 10 MeV region. The total-cross-section problems at lower energies do not persist into the scattering distributions at the energies of **Fig. V-A-2**. Finally, the general E potential (panel E) provides scattering distributions that are not as consistent with experimental observations as are those from potentials A or B. The latter was explicitly derived from holmium scattering data while potential E has a more generalized background.

Comparisons of measured and calculated (ROTM) inelastic neutron-scattering excitation functions were discussed in **Sec. III-C** and illustrated in **Fig. III-C-3**. That discussion points out that the evident over-prediction of inelastic-scattering excitation functions suggests that the β_2 deformations used in the above comparisons are perhaps 15% too large. It is not productive to test potentials in the context of inelastic scattering until the deformations are better known.

The above comparisons of measurements and calculations suggest that several general regional potentials will give reasonable calculational results. However, potentials developed for neighboring nuclei are not always suitable for quantitative results. One should be cautious when using regional or generalized potentials in this mass region. When highly quantitative results are sought there is no substitute for a solid experimental basis for the development of models for interpolation and extrapolation. In the case of rhenium, such a data base is very meager.

V-B. COMPARISONS WITH SOME EVALUATED FILES

There are a number of evaluated neutronic file systems for applications studies distributed around the world. Most of them are devoid of either elemental or isotopic rhenium evaluations, or utilize older versions of the ENDF/B files. This may reflect low world-wide interest in neutronic systems containing rhenium. The ENDF/B-VI system does have recently upgraded ^{185}Re and ^{187}Re isotopic evaluated neutronic files. These can be compared with relevant portions of the present work.

Elemental neutron total cross sections constructed from the ENDF/B-VI isotopic files are in very close agreement with what is experimentally known as, illustrated in **Fig. V-B-1**. The differences between measured and evaluated results is no more than several percent and then

largely in regions where the experimental values (particularly their energy dependencies) are suspect, as noted elsewhere herein. These evaluated and measured results are in very close (essentially exact) agreement with the above ROTM model, as shown. Minor differences between the model and the evaluation become evident only at energies approximately twice those of the present studies.

The present ROTM isotopic elastic-scattering is compared with the isotopic values of ENDF/B-VI in **Fig. V-B-2**. Over the energies of the present studies (below 10 MeV) the agreement between the present ROTM results and the isotopic values of ENDF/B-VI is within a few percent, or within the experimental uncertainties alone. Above approximately 10 - 12 MeV the isotopic extrapolation of the ROTM results in "elastic" cross sections that are increasingly larger than the evaluated quantities. As pointed out above, the present work is strictly valid only at energies of less than 10 MeV, and the present considerations assume only neutron total and scattering cross sections are significant. Well above 10 MeV, the latter assumption breaks down, for example at approximately 15 MeV the (n,2n) cross sections alone exceeds several barns. Thus it is not surprising that the evaluated elastic-scattering cross sections are smaller than those predicted by the present model well above 10 MeV. Comparisons of measured, calculated and evaluated inelastic-scattering cross sections are difficult due to the uncertain experimental cross sections and resolutions. However, ENDF/B-VI reasonably represents the inelastic-scattering cross sections of the first few excited states as illustrated in **Fig. V-B-2**. This result is bit surprising as most of the models use deformations that tend to over-predict the excitation of this first level of the g.s. rotational band, as illustrated in **Fig. III-C-3**. The rationale underlying the ENDF/B-VI evaluation is not known to the author. However, this particular inelastic-scattering cross section was already reasonably defined by the early experimental work of ref. (SGW68), well before the evaluation.

Possibly, in time some improvement of rhenium evaluations can be achieved through improved modeling and better understanding of neutron-reaction systematics in the rhenium mass region. However, major improvements are probably going to require some comprehensive measurements.

VI. CONCLUDING REMARK

There should be no misunderstanding, the experimental knowledge of the fast-neutron interaction with rhenium, and neighboring nuclei, is in very sorry shape. Even the total cross sections of rhenium are poorly known. Some of the desired measurements are difficult, but many of them involve the application of well-known techniques. The problem is that the facilities and professional skills necessary to provide the requisite information are vanishing, and even the limited knowledge available is fading. With this lack of experimental information, recourse is made to regional or global calculational models to provide information for applications. However, particularly in this deformed mass region, the results are very sensitive to nuclear structure effects. The models are most effective when they are used for interpolating between

measured values.

As in a number of other cases, the experimental knowledge of rhenium (p,n) and (p,p) processes is largely nonexistent, or is lost in the mists of time. This makes it difficult or impossible to assess some of the fundamental physical properties, particularly those dealing with iso-spin.

ACKNOWLEDGMENTS

The author would like to thank Drs. J. Raynal, P. Young and F. Kondev for their technical advice. The author is also indebted to the National Nuclear Data Center, Brookhaven Natl. Lab. for the efficient provision of essential nuclear data, and to Mr. J. Bolling and associates for providing the computation facilities used in much of this work.

IN MEMORIAM

This is the first report in this ANL/NDM series since the passing of R. J. Howerton. The professional community is very much indebted to Bob Howerton for his many contributions to nuclear data endeavors. He was a frequent contributor to this report series. He will be very missed by those many who owe so much to him, including the author.

REFERENCES

- (Bau+82) M. Bauer et al., J. Phys. **G8** 525 (1982).
- (BFG69) C. Batty, E. Friedman and G. Greenlees, Nucl. Phys. **A127** 368 (1969).
- (BG69) F. Becchetti Jr., and G. Greenlees, Phys. Rev. **182** 1190 (1969).
- (BDS79) G. Brown, J. Dehesa and J. Speth, Nucl. Phys. **A330** 290 (1979).
- (Chi+90) S. Chiba, P. Guenther, R. Lawson and A. Smith Phys. Rev. **C42** 2487 (1990).
- (CL55) L. Cranberg and J. Levin, **Proc. Conf. on Peaceful Uses of Atomic Energy** Geneva, United Nations Press (1958).
- (Com79) J. Comfort, Phys. Rev. Lett. **42** 30 (1979).
- (CSL83) Editors:- H. Conde, A. Smith and A. Lorenz, Nuclear Standards File, **IAEA Tech. Report 227** (1983).
- (Dro87) M. Drog, IAEA Report **IAEA-TECDOC-410** (1987).
- (ENDF/B) Evaluated Nuclear Data File/B-VI, National Nuclear Data Center, Brookhaven Natl. Lab.
- (FCR72) J. Ferrer, J. Carlson and J. Rapaport, Nucl. Phys. **A275** 325 (1977).
- (Fes58) H. Feshbach, Ann. Rev. Nucl. Sci. **8** 49 (1958).

- (GC65) A. Gilbert and A. Cameron, *Can. J. Phys.* **43** 1446 (1965).
- (GMP70) G. Greenlees, W. Makofske and G. Pyle, *Phys. Rev.* **C1** 1145 (1970).
- (GPA72) U. Goetz, H. Pauli and K. Adler, *Nucl. Phys.* **A192** 1 (1972).
- (GPT68) W. Greenlees, G. Pyle and Y. Tang, *Phys. Rev.* **171** 1115 (1968); also *Phys. Rev.* **C1** 1145 (1970).
- (Hod63) P. Hodgson, **The Optical Model of Elastic Scattering** Clarendon, Oxford (1963).
- (Hod94) P. Hodgson, **The Nucleon Optical Model** World Sci. Pub., Singapore (1994).
- (HW72) B. Holmqvist and T. Wiedling, *Nucl. Phys.* **A188** 24 (1972).
- (KD03) A. Koning and J. Delaroche, *Nucl. Phys.* **A713** 231 (2003).
- (Lan+61) R. Lane et al., *Ann. Phys.* **12** 135 (1961).
- (Lan62) A. Lane, *Nucl. Phys.* **35** 676 (1962); also *Phys. Rev. Lett.* **8** 171 (1962).
- (LGS87) R. Lawson, P. Guenther and A. Smith, *Phys. Rev.* **C36** 1298 (1987).
- (Lip66) R. Lipperheide, *Nucl. Phys.* **89** 97 (1966).
- (LS01) R. Lawson and A. Smith, Argonne Natl. Lab. Report **ANL/NDM-152** (2001).
- (MN59) B. Mottelson and S. Nilsson, *Kgl. Danske Videnskab Selskab. Mat. Fys. Skrifter* **1** 8 (1959).
- (MN81) C. Mahaux and H. Ngo, *Phys. Lett.* **100B** 285(1981).
- (Mol80) P. Moldauer, *Nucl. Phys.* **A344** 185 (1980).
- (MY87) R. Macklin and P. Young, *Nucl. Sci. and Eng.* **97** 239 (1987).
- (NNDC) National Nuclear Data Center, Brookhaven Natl. Lab.
- (Pas67) G. Passatore, *Nucl. Phys.* **A95** 694 (1967).
- (PB62) F. Perey and B. Buck, *Nucl. Phys.* **32** 353 (1962).
- (Pre62) M. Preston, **Physics of the Nucleus** Addison-Wesley, Reading, MA (1962).
- (Ray96) J. Raynal, The Coupled Channels Code **ECIS96**, private communication, see also CEA Report **CEA-N-2772** (1994).
- (Sat69) G. Satchler, **Iso-spin in Nuclear Physics**, ed. D. Wilkinson, North-Holland, Amsterdam (1969).
- (Sat83) G. Satchler, **Direct Nuclear Reactions** Addison-Wesley, Reading, MA (1983).
- (SGW68) A. Smith, P. Guenther and J. Whalen, *Phys. Rev.* **168** 1344 (1968).
- (Smi90) A. Smith, **Argonne Memorandum** (1990), unpublished.
- (Smi92) A. Smith, Argonne Natl. Lab. Report **ANL/NDM-127** (1992); see also *Phys. Rev.* **C45** 1260 (1992); *Z. Phys.* **A360** 265 (1982); *Nucl. Instr. and Methods* **50** 277 (1977); and references cited therein.
- (Smi98) A. Smith, *J. Phys.* **G24** 637 (1998).
- (Smi99) A. Smith, Argonne Natl. Lab. Report **ANL/NDM-147** (1999).
- (Smi99A) A. Smith, Argonne Natl. Lab. Report **ANL/NDM-142** (1999).
- (Smi00) A. Smith, Argonne Natl. Lab. Report **ANL/NDM-151** (2000); also A. Smith, *Ann. Nucl. Energy* **28** 1745 (2001).
- (Smi01) A. Smith, Argonne Natl. Lab. Report **ANL/NDM-153** (2001); also A. Smith, *Ann. Nucl. Energy* **29** 1241 (2002).
- (Tam65) T. Tamura, *Rev. Mod. Phys.* **37** 679 (1965).
- (Tul90) J. Tuli, **Nuclear Wallet Cards**, National Nuclear Data Center, Brookhaven Natl.

- Lab. (1990).
- (WG86) R. Walter and P. Guse, **Proc. of Conf. on Nucl. Data for Basic and Applied Sci.** Eds. P. Young et al., 2 272, Gordon and Breach, New York (1986).
- (Wol51) L. Wolfenstein, *Phys. Rev.* **82** 690 (1951).
- (You86) P. Young, Los Alamos Natl. Lab. Report **LA-10689-PR** (1986).

APPENDICES

A-1. PRIOR NEUTRON TOTAL-CROSS-SECTION DATA

There are only five references giving neutron total cross sections of rhenium or its isotopes that are relevant to the present considerations. These results are illustrated in **Fig. A-1**. Given the sparsity of experimental information, the experimental results are qualitatively consistent within themselves and with the ENDF/B-VI evaluation. However, it would be well to have several verification measurements below energies of approximately 15 MeV, and nothing seems to be known at higher energies. All of the relevant results from the literature are for elemental rhenium.

(SMS76) D. Stupegia, A. Madson and M. Schmidt, private communication, 1976 (*12125, asterisks denote EXFOR numbers). Many monoenergetic-source results extending from approximately 10 keV to 1.9 MeV. Resolutions 10-20 keV.

(TS68) R. Tabony and K. Seth, *Ann. Phys.* **46** 401, 1968 (*11953). Many monoenergetic results extending from approximately 30 to 650 keV. Resolution several keV.

(SGW68) A. Smith, P. Guenther and J. Whalen, *Phys. Rev.* **168** 1344, 1968 (*10631). Many monoenergetic results extending from approximately 0.5 to 1.5 MeV. Resolution a few keV.

(DV72) W. Dilg and H. Vonach, *EANDC(E)-150* 40, 1972 (*20583). A single value at 3 keV.

(FG71) D. Foster and D. Glasgow, *Phys. Rev.* **C3** 576, 1971 (*10047). Detailed white-source results with many values distributed between approximately 2.2 and 14.9 MeV.

A-2. PRIOR NEUTRON ELASTIC-SCATTERING DATA

There appear to be only two measurements of neutron "elastic" scattering from rhenium or its isotopes; 1) A. Smith, P. Guenther and J. Whalen, *Phys. Rev.* **168** 1344, 1968 (*10631); and 2) V. Nikolenko, A. Popov and G. Samosvat, *INR-P3* **85** 133, 1985 (*40937); again, numbers preceded by the asterisk are EXFOR reference numbers). The former gives comprehensive coverage from 0.3 to 1.5 MeV with a number of scattered-neutron angular distributions. The latter reference presents some low-energy pulsed-reactor data and only very fragmentary

differential information at approximately 450 keV. Before the present results, knowledge of “elastic” neutron scattering from rhenium or its isotopes was essentially limited to the energy range 0.3 - 1.5 MeV and one set of measurements.

A-3. PRIOR NEUTRON INELASTIC-SCATTERING DATA

Prior measurement of neutron inelastic scattering from rhenium and/or its isotopes is limited to one reference; A. Smith, P. Guenther and J. Whalen, *Phy. Rev.* **168** 1344, 1968 (*10631). That work is more than 35 years old and confined to incident energies of less than 1.6 MeV. Interestingly, that early inelastic-scattering work suggested shortcomings in the contemporary knowledge of the excited structure of rhenium, particularly ^{185}Re . These deficiencies have been largely removed through later structure work, as summarized in the Nuclear Data Sheets.

TABLES

Table III-A-1:- Parameters for the SOM potential. Particle energies (E) and potential strengths (V and W) are given in MeV and geometries in fermis. Approximate strengths in volume-integrals-per-nucleon (J) are in units of MeV-fm³. This is entirely an iso-scalar potential:- i.e., $V_1=W_1=0$ of Eq. III-B-1.

Real Potential

Strength

$$V = 45.931 - 0.04937 \cdot E$$

$$J_v \approx 380.02 - 0.4085 \cdot E$$

Reduced Radius

$$r_v = 1.2196$$

Diffuseness

$$a_v = 0.6607$$

Imaginary Potential

Strength

$$W = 14.713 - 1.9038 \cdot E, \text{ for } E \text{ less than } 5.62 \text{ MeV}$$

$$J_w \approx 79.18 - 8.73 \cdot E$$

$$W = 2.0750 + 0.34392 \cdot E, \text{ for } E \text{ greater than } 5.62 \text{ MeV}$$

$$J_w \approx 11.17 + 3.91 \cdot E$$

Reduced Radius

$$r_w = 1.3384$$

Diffuseness

$$a_w = 0.3391 + 0.02293 \cdot E$$

Spin-Orbit Potential (WG86)

Strength

$$V_{so} = 6.157 - 0.015 \cdot E$$

Reduced Radius

$$r_{so} = 1.103$$

Diffuseness

$$a_{so} = 0.56$$

Table III-B-1:- Parameters for the SOMV potential. Particle energies (E) and potential strengths (V and W) are given in MeV and geometries in fermis. Approximate strengths in volume-integrals-per-nucleon (J) are in units of MeV· fm³. This is an iso-vector potential with V₁=16 MeV and W₁ = 8 MeV.

Real Potential

Strength

$$V = 49.930 + 0.20568 \cdot E$$

$$J_V \approx 385.78 + 1.5892 \cdot E$$

Reduced Radius

$$r_v = 1.1920$$

Diffuseness

$$a_v = 0.6467$$

Imaginary Potential

Strength

$$W = 14.245 - 1.5217 \cdot E, \text{ for } E \text{ less than } 6.165 \text{ MeV}$$

$$J_W \approx 78.74 - 5.78 \cdot E$$

$$W = 3.6126 + 0.20257 \cdot E, \text{ for } E \text{ greater than } 6.165 \text{ MeV}$$

$$J_W \approx 19.97 + 4.19 \cdot E$$

Reduced Radius

$$r_v = 1.3409$$

Diffuseness

$$a_w = 0.3469 + 0.03291 \cdot E$$

Spin-Orbit Potential is as given in **Table III-A-1** (WG86).

Table III-B-2:- Parameters for the SOMV potential. Particle energies (E) and potential strengths (V and W) are given in MeV and geometries in fermis. Approximate strengths in volume-integrals-per-nucleon (J) are in units of MeV-fm³. This is an iso-vector potential with V₁ = 24 MeV and W₁ = 12 MeV.

Real Potential

Strength

$$V = 51.729 + 0.23137 \cdot E$$

$$J_V \approx 392.59 + 1.7560 \cdot E$$

Reduced Radius

$$r_v = 1.1864$$

Diffuseness

$$a_v = 0.6286$$

Imaginary Potential

Strength

$$W = 16.796 - 1.8332 \cdot E, \text{ for } E \text{ less than } 6.27 \text{ MeV}$$

$$J_w \approx 89.57 - 5.917 \cdot E$$

$$W = 4.1190 + 0.19007 \cdot E, \text{ for } E \text{ greater than } 6.27 \text{ MeV}$$

$$J_w \approx 21.96 + 4.90 \cdot E$$

Reduced Radius

$$r_w = 1.3542$$

Diffuseness

$$a_w = 0.3284 + 0.03822 \cdot E$$

Spin-Orbit Potential is the same as give in **Table III-A-1.** (WG86)

Table III-C-1:- Parameters for the elemental rotational coupled-channels model (ROTM) potential. Particle energies (E) and potential strengths (V and W) are given in MeV and geometries in fermis. Approximate strengths in volume-integrals-per-nucleon (J) are in units of MeV-fm³.

Real Potential

Strength

$$V = 48.218 - 0.33286 \cdot E$$

$$J_V \approx 430.16 - 2.9694 \cdot E$$

Reduced Radius

$$r_v = 1.2446$$

Diffuseness

$$a_v = 0.6035$$

Imaginary Potential

Strength

$$W = 2.7928 + 0.34516 \cdot E$$

$$J_w \approx 18.27 + 2.2580 \cdot E$$

Reduced Radius

$$r_w = 1.2934$$

Diffuseness

$$a_w = 0.4376$$

Spin-Orbit Potential is the same as that of **Table III-A-1** (WG86)

Deformations

$$^{185}\text{Re} \quad \beta_2 = 0.22 \quad \beta_4 = -0.085$$

$$^{187}\text{Re} \quad \beta_2 = 0.21 \quad \beta_4 = -0.085$$

Table III-C-2:- Parameters for the ^{187}Re rotational potential, as described in the text. The nomenclature is the identical to that of **Table III-C-1**.

Real Potential

Strength

$$V = 48.934 - 0.3638 \cdot E$$

$$J_v \approx 428.2 - 3.184 \cdot E$$

Reduced Radius

$$r_v = 1.2366$$

Diffuseness

$$a_v = 0.6011$$

Imaginary Potential

Strength

$$W = 2.5507 + 0.36422 \cdot E$$

$$J_w \approx 16.53 + 2.3561 \cdot E$$

Reduced Radius

$$r_w = 1.2603$$

Diffuseness

$$a_w = 0.4557$$

Spin-Orbit Potential is the same as that of **Table III-A-1** (WG86)

Deformations are same as **Table III-C-1**

Table III-C-3. Correlation of observed inelastic-scattering excitation energies in MeV (Column A) with reported (NNDC) excitations in ^{185}Re (Column B) and in ^{187}Re (Column C).

No.	Column A.	Column B	Column C
0	0.0	0.0, 5/2+	0.0, 5/2+
1	0.130	0.125, 7/2+	0.134, 7/2+
2	0.214	-----	0.206, 9/2-
3	0.295	0.284, 9/2+	0.303, 9/2+
4	0.386	0.368, 9/2-	0.390, 11/2-
5	0.505	0.475, 11/2+ 0.547, 11/2-	0.511, 1/2+
6	0.635	0.646, 1/2+	0.582, 5/2+ 0.589, 3/2+ 0.618, 3/2+ 0.625, 1/2+ 0.647, 5/2+

Table III-D-1:- Parameters for the SOM potential with dispersive contributions, as described in the text. The nomenclature is identical to that of **Table III-A-1**.

Real Potential

Strength

$$V = 43.587 - 0.61101 \cdot E$$
$$J_V \approx 321.14 - 4.5017 \cdot E$$

Reduced Radius

$$r_v = 1.1802$$

Diffuseness

$$a_v = 0.6549$$

Imaginary Potential

Strength

$$W = 22.754 - 3.3575 \cdot E, \text{ for } E \text{ less than } 5.72 \text{ MeV}$$
$$J_W \approx 85.22 - 8.53 \cdot E$$
$$= 1.5256 + 0.35369 \cdot E, \text{ for } E \text{ greater than } 5.72 \text{ MeV}$$
$$J_W \approx 14.40 + 3.848 \cdot E$$

Reduced Radius

$$r_w = 1.3361$$

Diffuseness

$$a_w = 0.2742 + 0.03234 \cdot E$$

Spin-Orbit Potential the same as given in **Table III-A-1**. (WG86)

Table III-D-2:- Parameters for the ROTM with dispersive contributions, as described in the text. The nomenclature is identical to that of **Table III-C-1**.

Real Potential

Strength

$$V = 48.199 - 0.30699 \cdot E$$

$$J_V \approx 411.68 - 2.6469 \cdot E$$

Reduced Radius

$$r_V = 1.2277$$

Diffuseness

$$a_V = 0.5768$$

Imaginary Potential

Strength

$$W = 3.2946 + 0.34156 \cdot E$$

$$J_W \approx 20.13 + 2.0869 \cdot E$$

Reduced Radius

$$r_W = 1.2734$$

Diffuseness

$$a_W = 0.4217$$

Spin-Orbit Potential is the same as that of **Table III-A-1**. (WG86)

Deformations as per **Table III-C-1**.

Fig. II-1. Measured elemental Re differential-scattering cross sections. The experimental values are noted by symbols and curves indicate the results of fitting the measured values with legendre-polynomial expansions. Incident neutron energies, in MeV, are numerically noted. Throughout this work data are presented in the laboratory coordinate system.

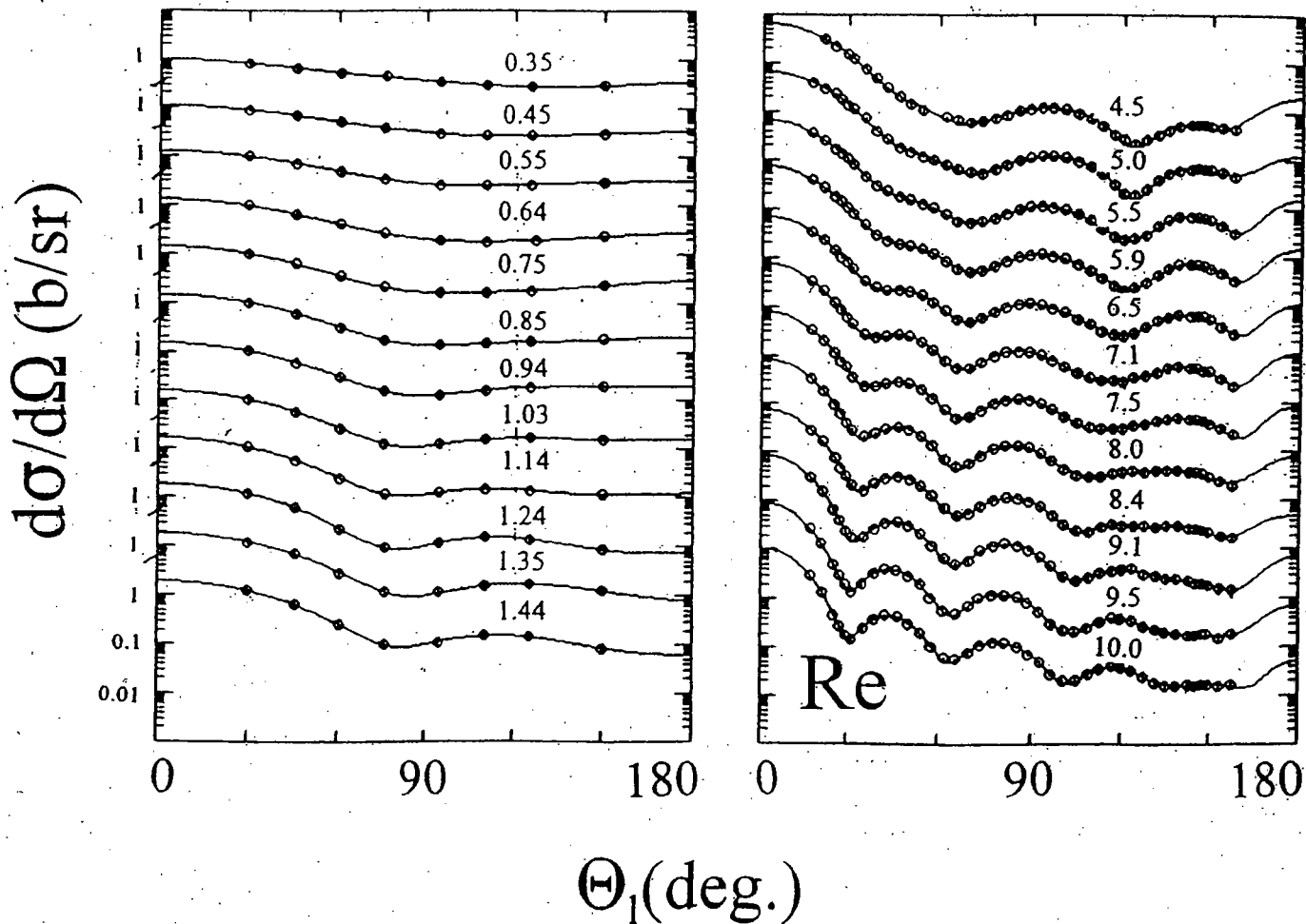


Fig. III-A-1. Comparison of measured (symbols) and SOM-calculated (curve) neutron total cross section of elemental rhenium.

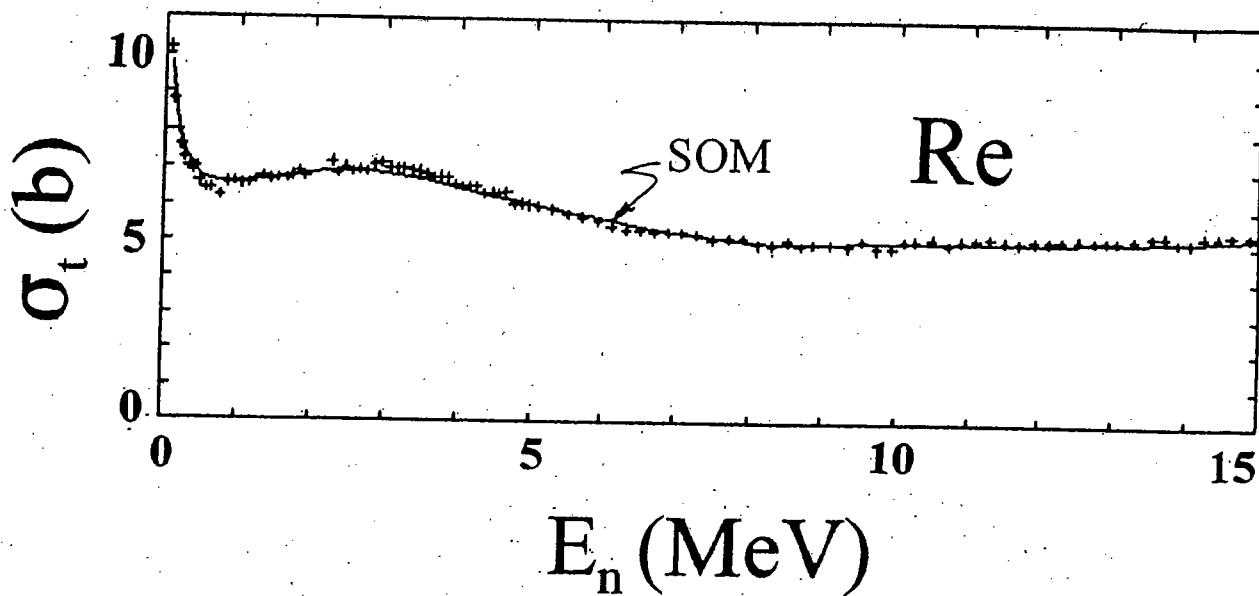


Fig. III-A-2. Comparisons of measured (symbols) and SOM-calculated (curves) scattered-neutron "elastic" distributions (curves) of elemental rhenium. Incident-neutron energies are numerically noted in MeV.

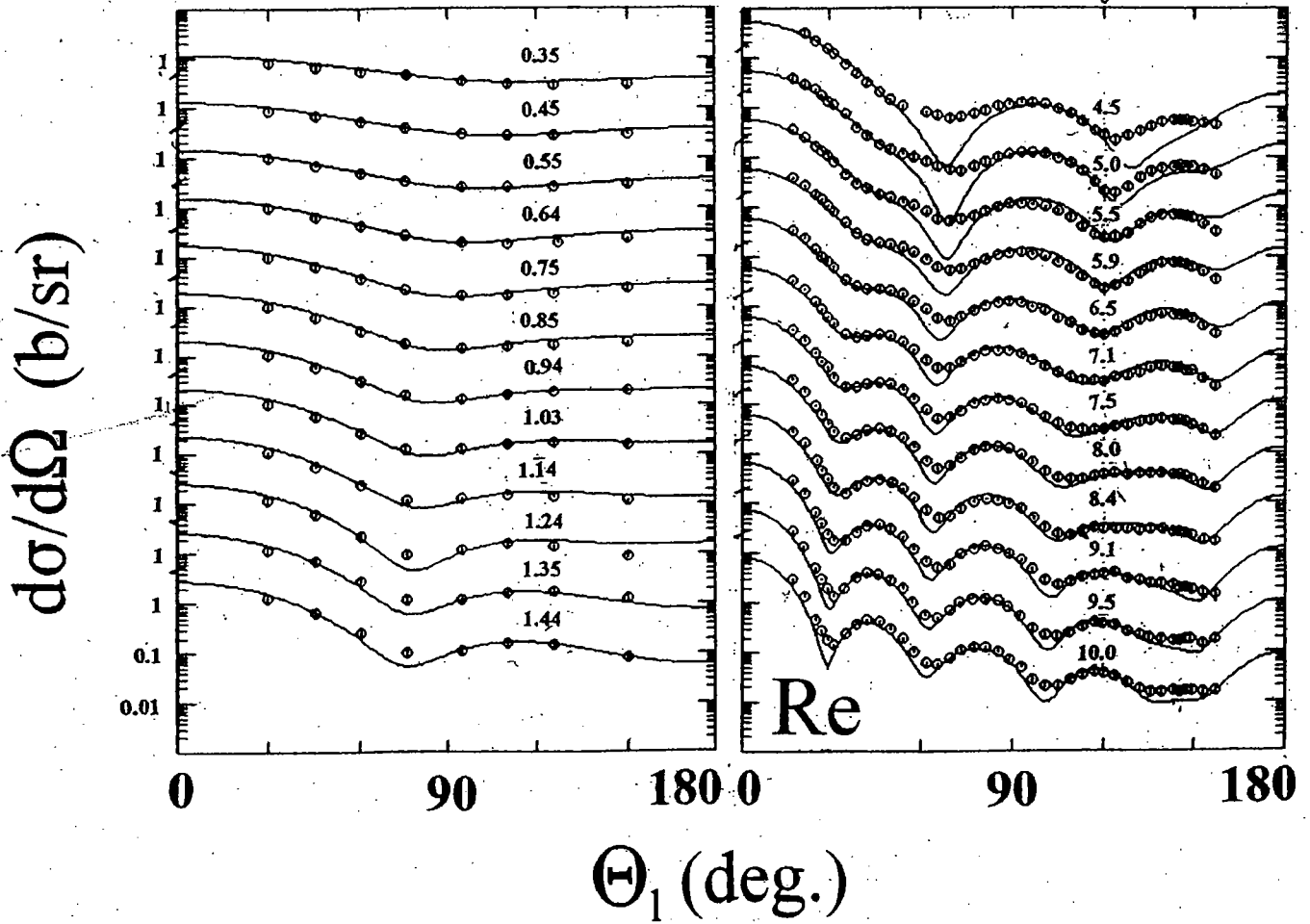


Fig. III-B-1. Measured (symbols) and calculated (curve) total cross sections of elemental rhenium. The calculations are based upon the SOMV potential of **Table III-B-1**. $V_1/W_1 = 16/8$ MeV.

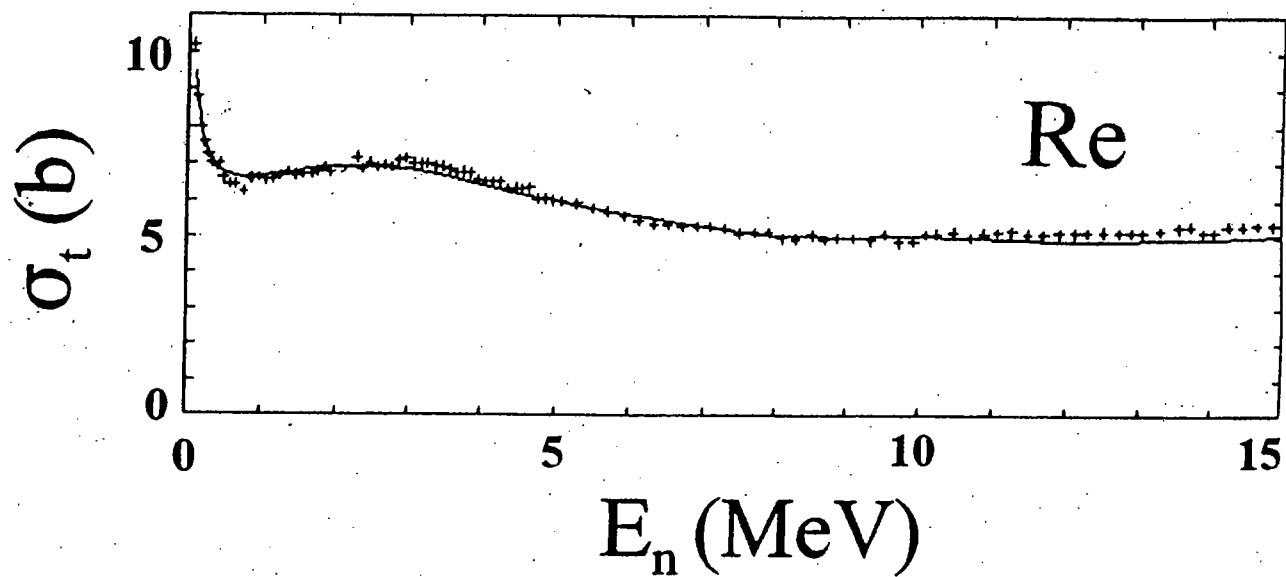


Fig. III-B-2. Measured (symbols) and calculated (curves) differential "elastic" scattering from elemental Re. The calculations used the SOMV potential of Table III-B-1 with $V_1/W_1 = 16/8$ MeV.

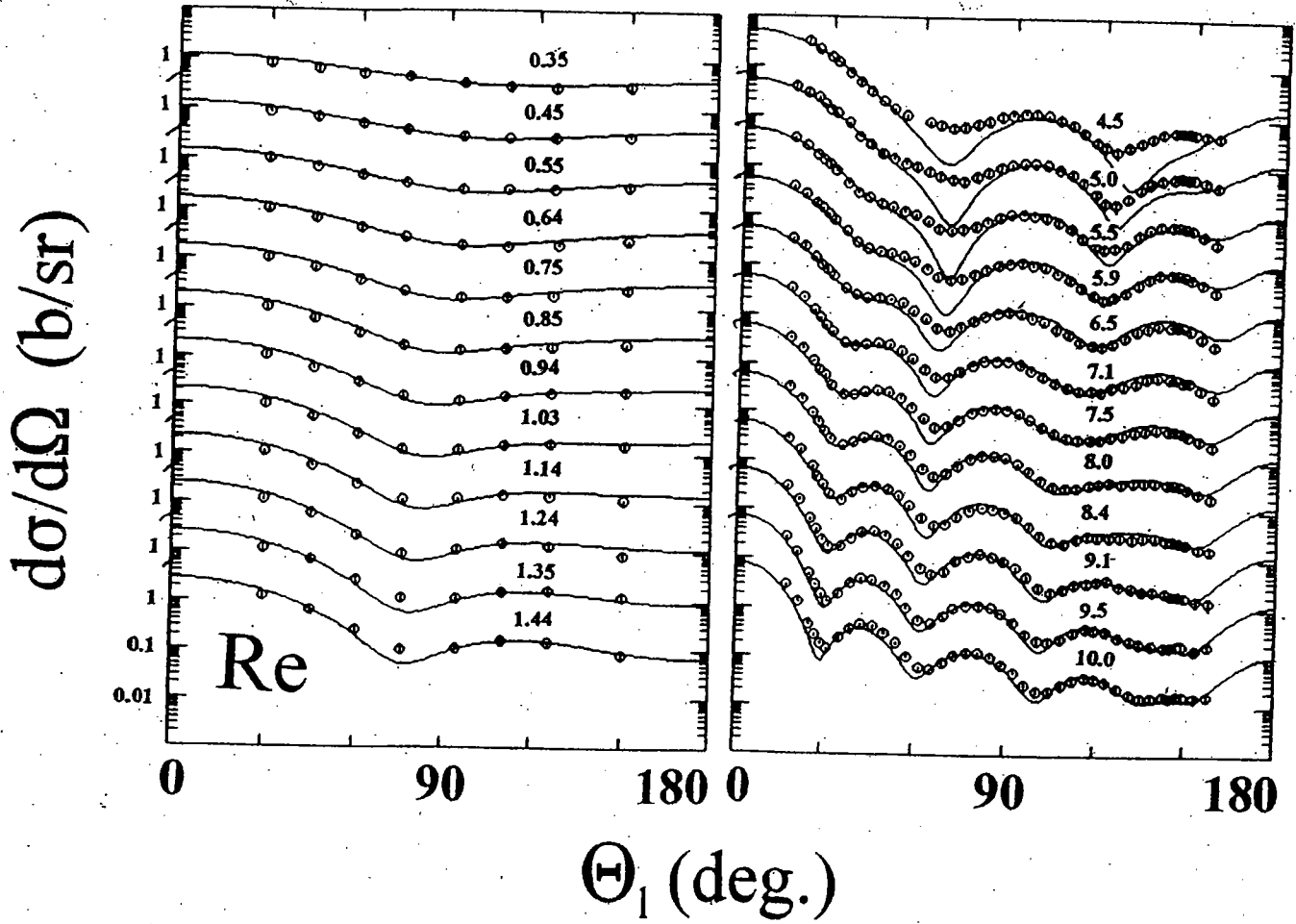


Fig. III-C-1. Comparison of measured (symbols) and ROTM-calculated (curve) neutron total cross section of elemental rhenium. The calculations employed the elemental potential of Table III-C-1, as described in the text.

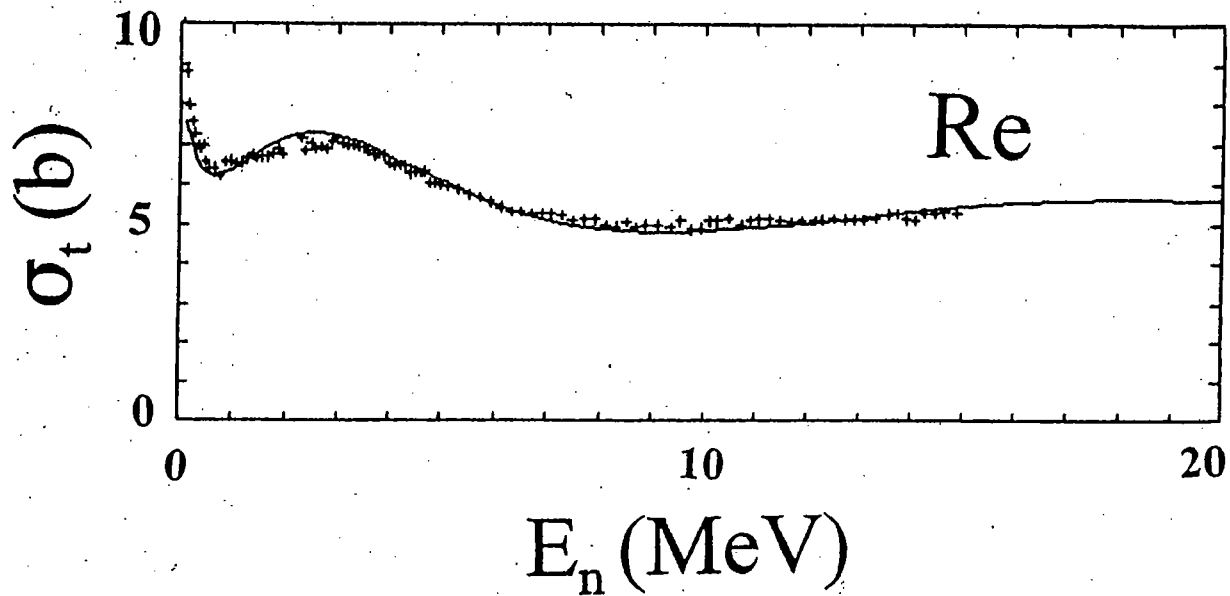


Fig. III-C-2. Comparison of measured (symbols) and calculated (curves) scattering distributions of elemental rhenium. The calculations employed the ROTM of Table III-C-1. Incident neutron energies are numerically cited. A single curve at a given energy represents simple calculated elastic scattering. At energies with two curves, the elastic (lower) and elastic+first-inelastic excitation of the g.s. rotational band (upper) are represented. At energies with three curves, the first represents simple calculated elastic scattering (lower), the second the elastic+first inelastic distribution, and the third the elastic+the first two inelastic contributions from the g.s. rotational band.

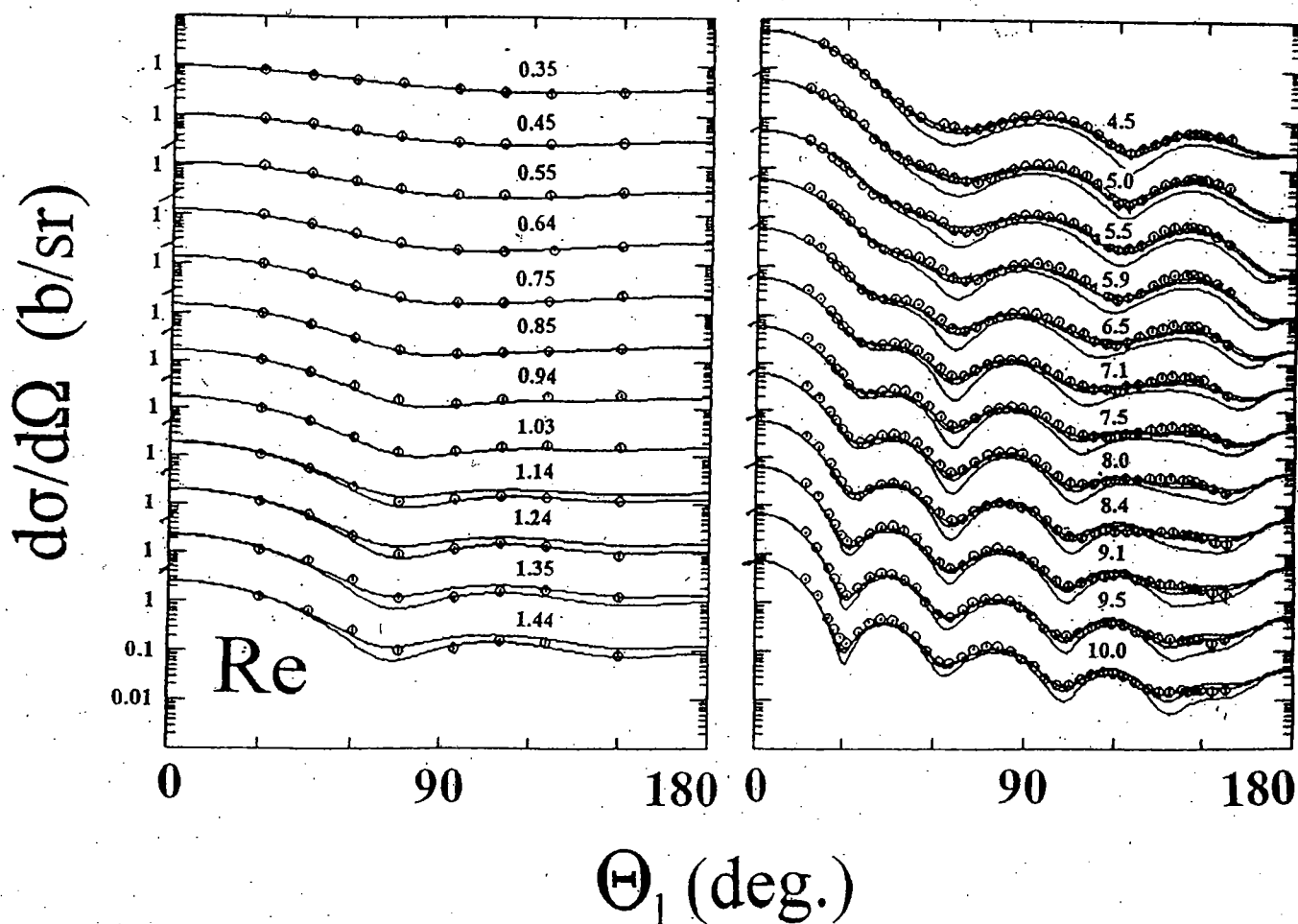


Fig. III-C-3. Measured (symbols) and calculated (curves) inelastic-excitation cross sections of elemental rhenium. The calculations were based upon the ROTM potential of **Table III-C-1**. The excitation energies 1 through 6 are correlated with reported level structure in the two isotopes of rhenium in **Table III-C-3**.

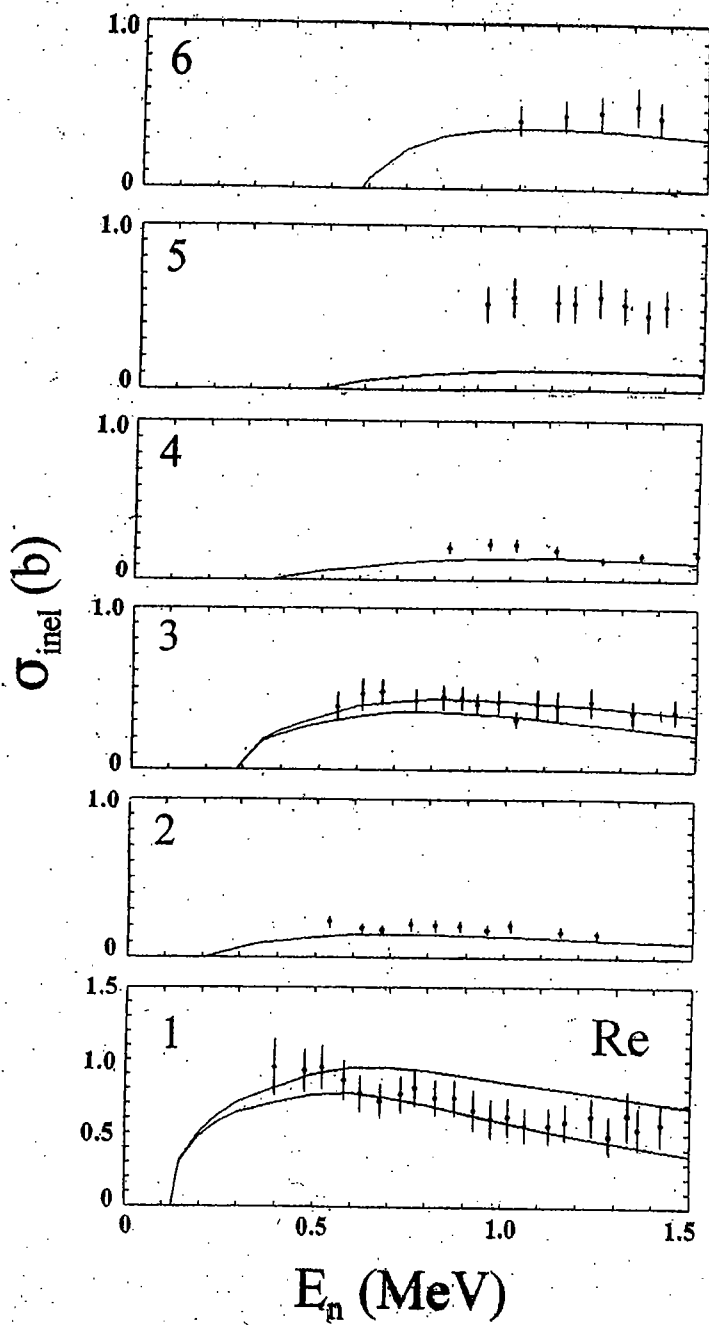


Fig. III-C-4. Comparison of measured (symbols) and calculated (curve) cross sections for the inelastic neutron excitation of the first excited levels in the two isotopes making up elemental rhenium. The calculations used the reduced β_2 deformations and associated parameters as discussed in the text.

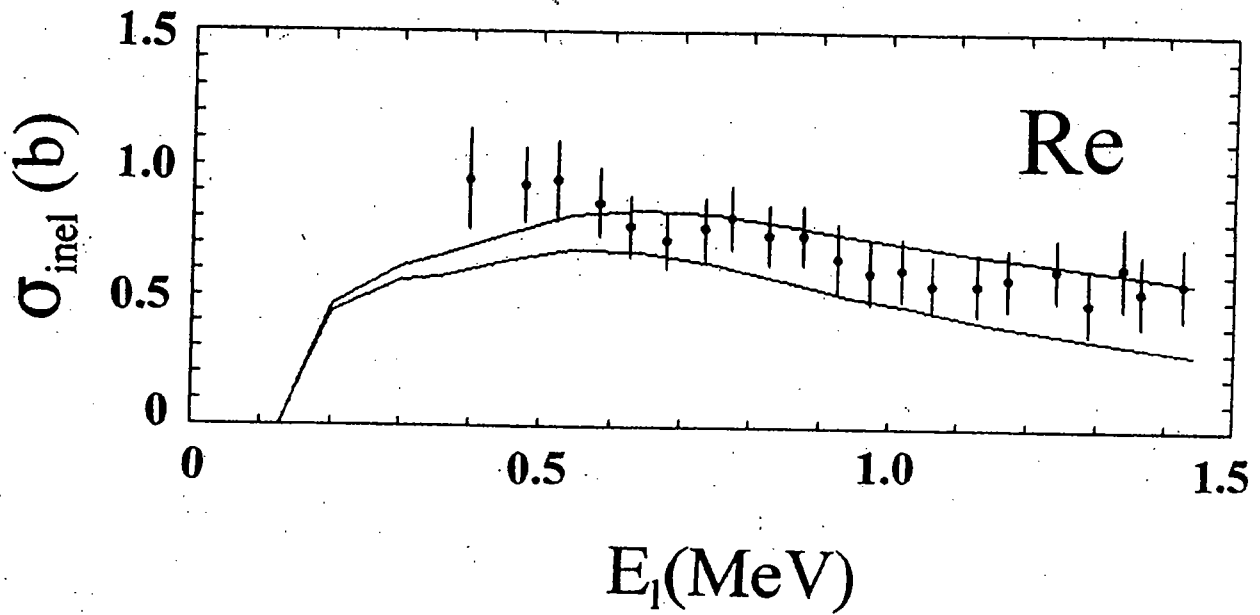


Fig. III-D-1. The fraction of the imaginary potential strength (DISP) that will be reflected into the real potential. These are the values of the ratio $\Delta J_{\text{sur}}/J_w$ of Eq. III-D-2 as a function of energy.

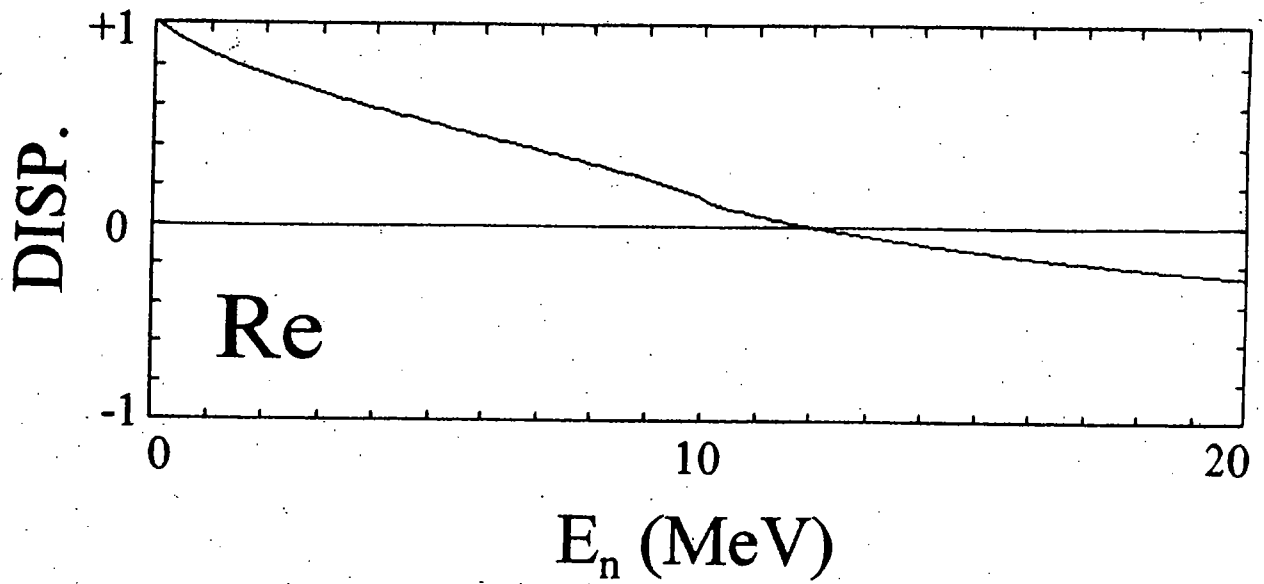


Fig. III-D-2. Comparison of measured (symbols) and calculated (curve) total cross sections of elemental rhenium. The calculations used the dispersive potential of Table III-D-1.

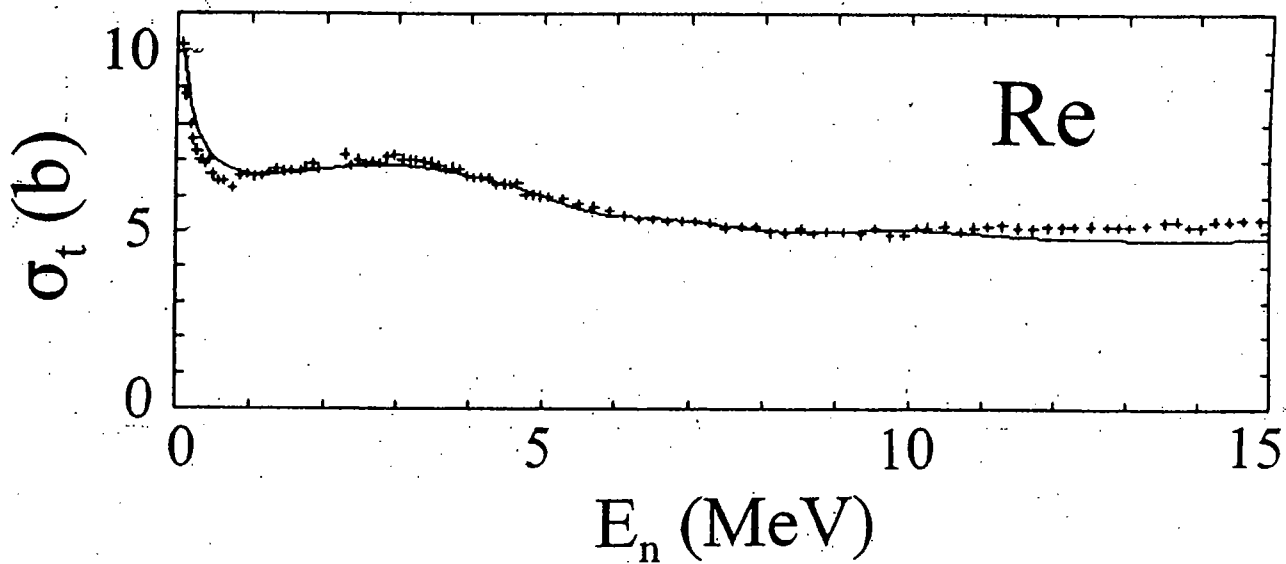


Fig. III-D-3. Comparison of measured (symbols) and calculated (curve) total cross section of elemental rhenium. The calculations used the dispersive rotational potential of Table III-D-2.

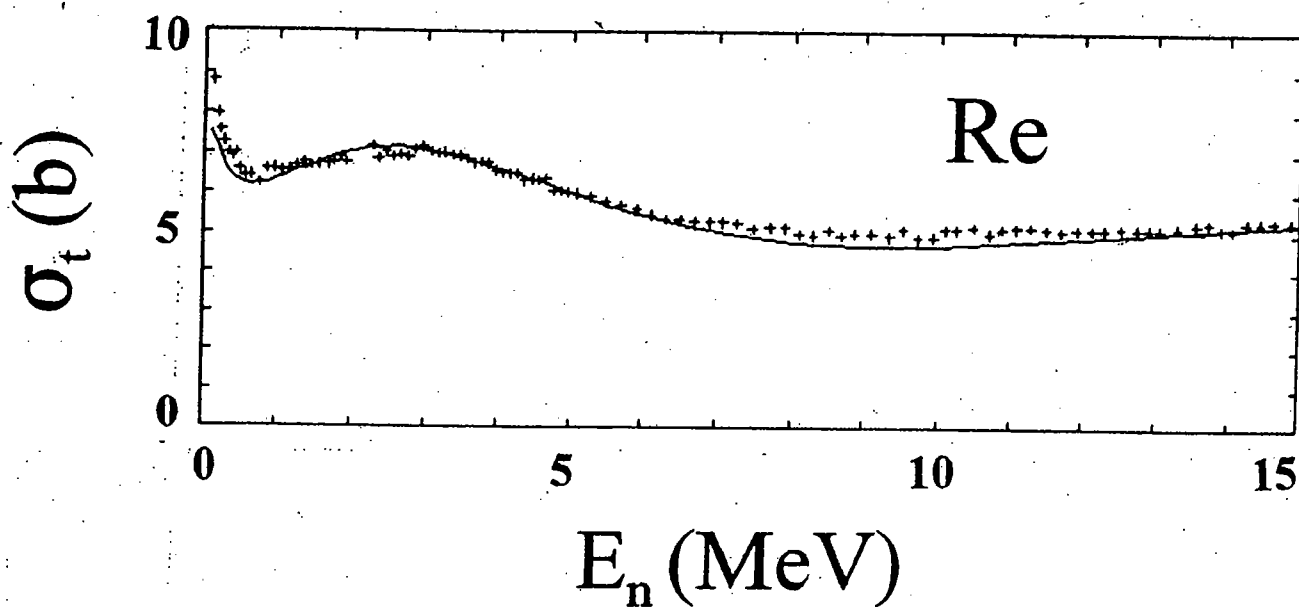


Fig. III-D-4. Comparison of measured (symbols) and calculated (curves) differential "elastic" scattering of elemental rhenium. The calculations used the dispersive rotational potential of Table III-D-2. The nomenclature of the figure is similar to that of Fig. III-C-2.

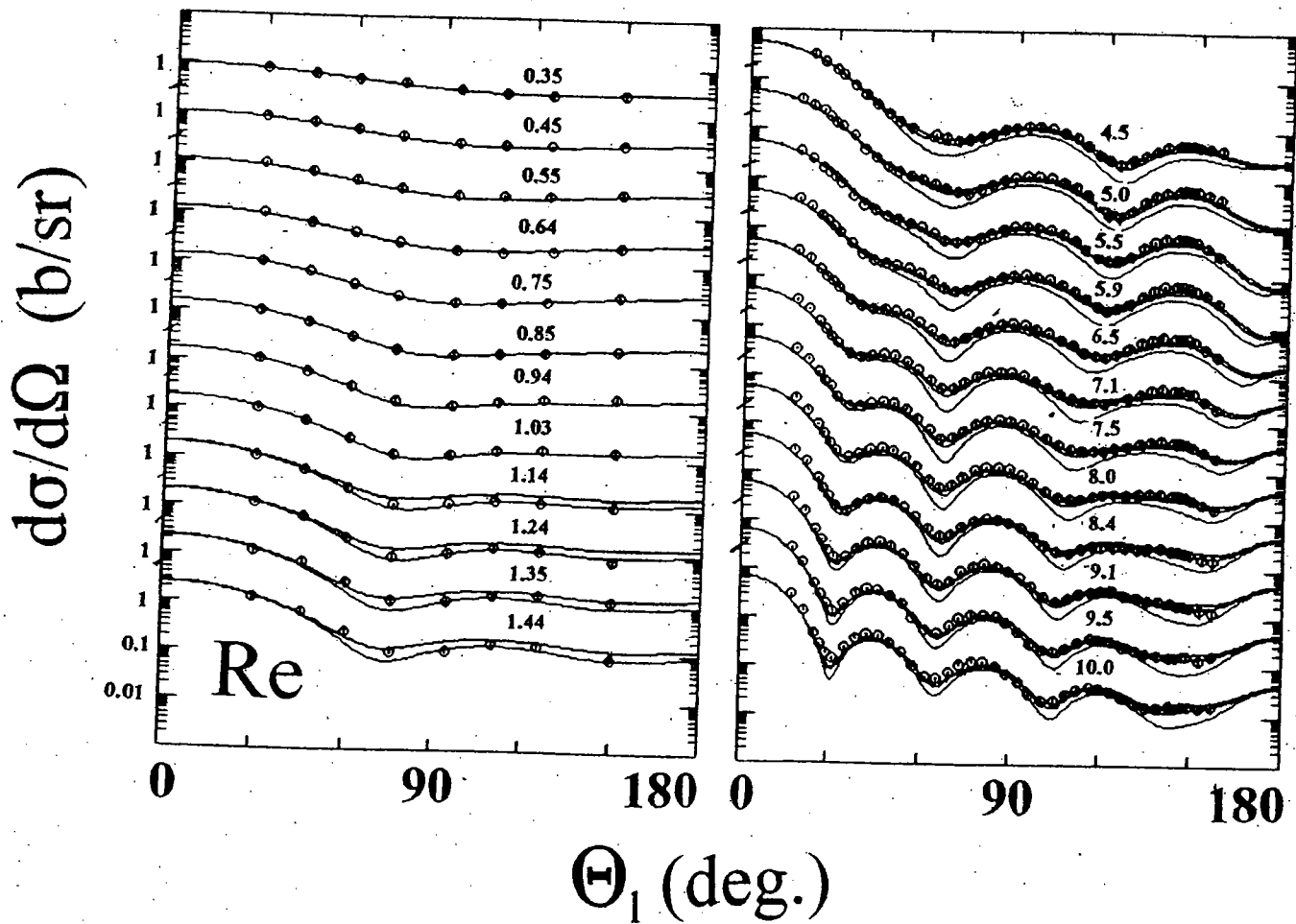


Fig. V-A-1. Illustrative comparisons of measured (symbols) and calculated (curves) neutron total cross sections of elemental rhenium. Sections A to E of the figure correspond to potential variants discussed in the text.

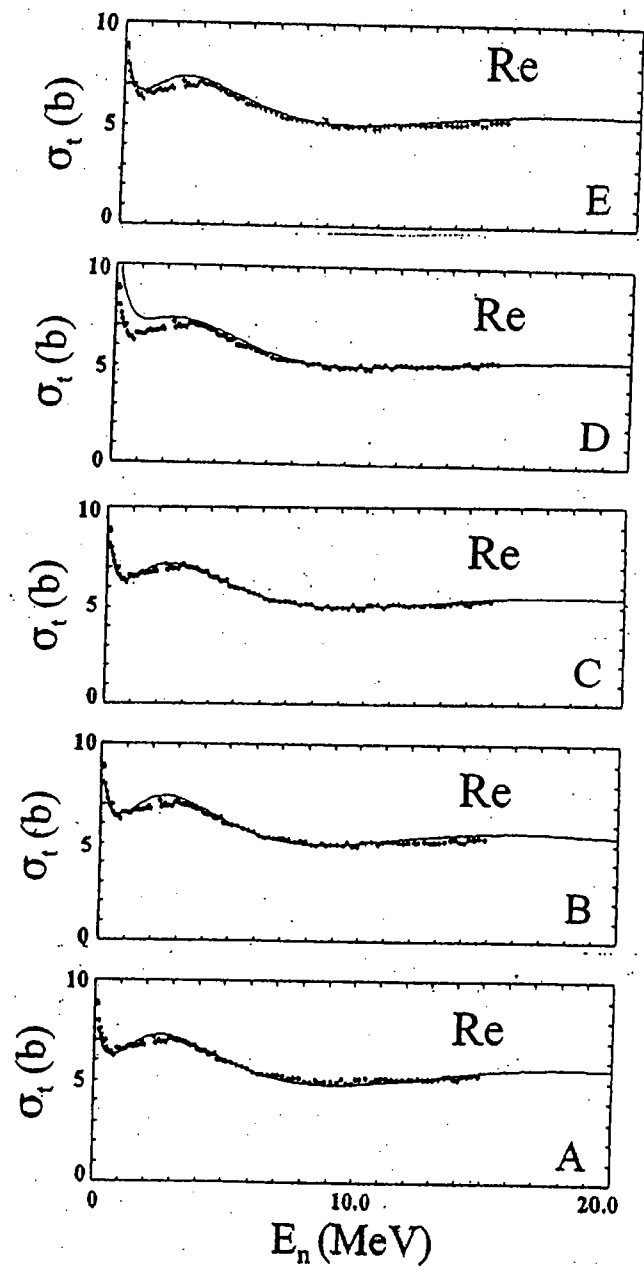


Fig. V-A-2. Comparisons of measured (symbols) and calculated (curves) differential-scattering distributions. Panels A through E correspond to the potentials defined and discussed in the text. The nomenclature of the figure is identical to that of Fig. III-C-2.

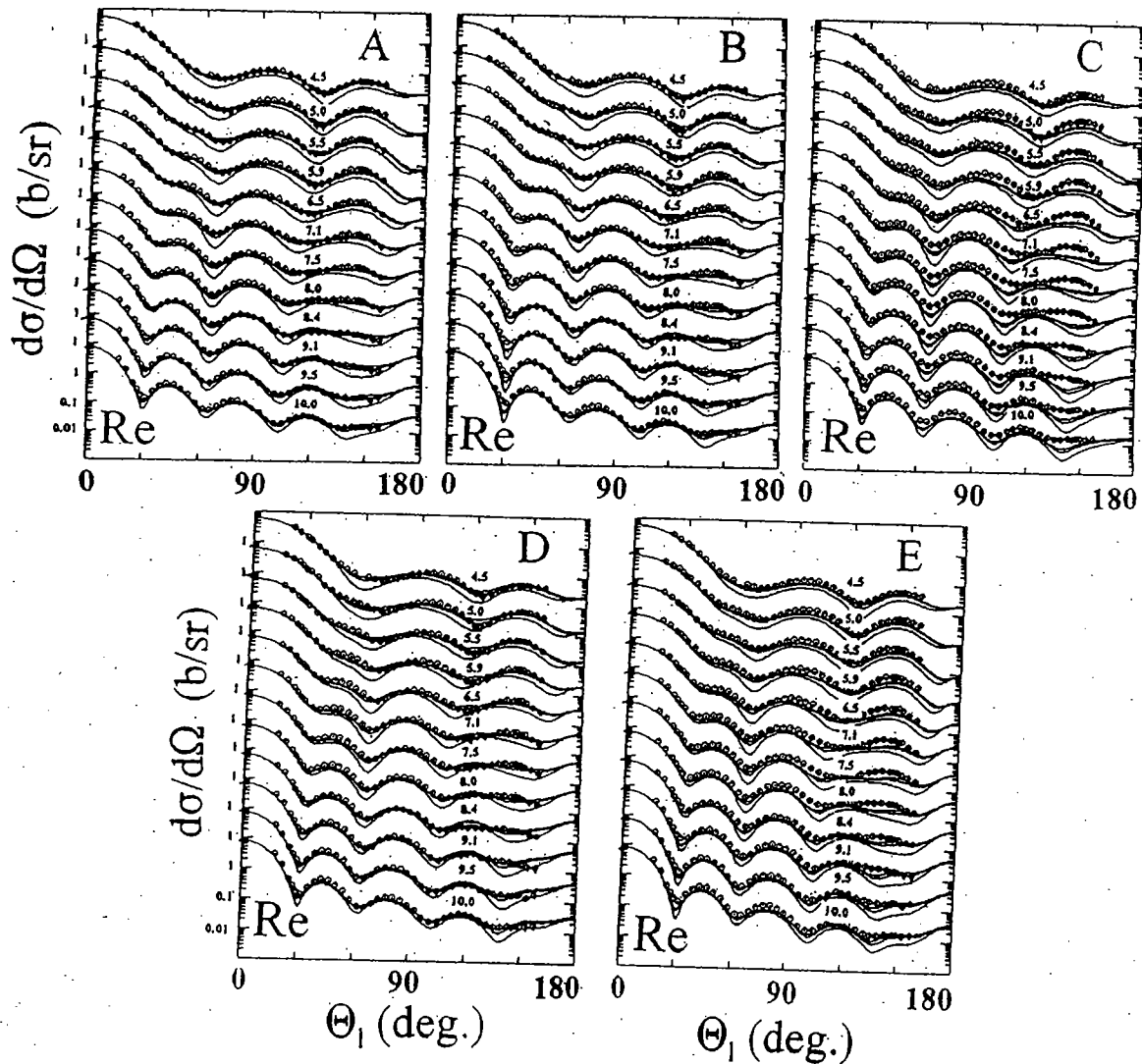


Fig. V-B-1. Comparison of measured ("+" symbols), calculated (ROTM, curve with "x" symbols), and ENDF/B-VI evaluated (curve with "o" symbols) neutron total cross sections of elemental rhenium.

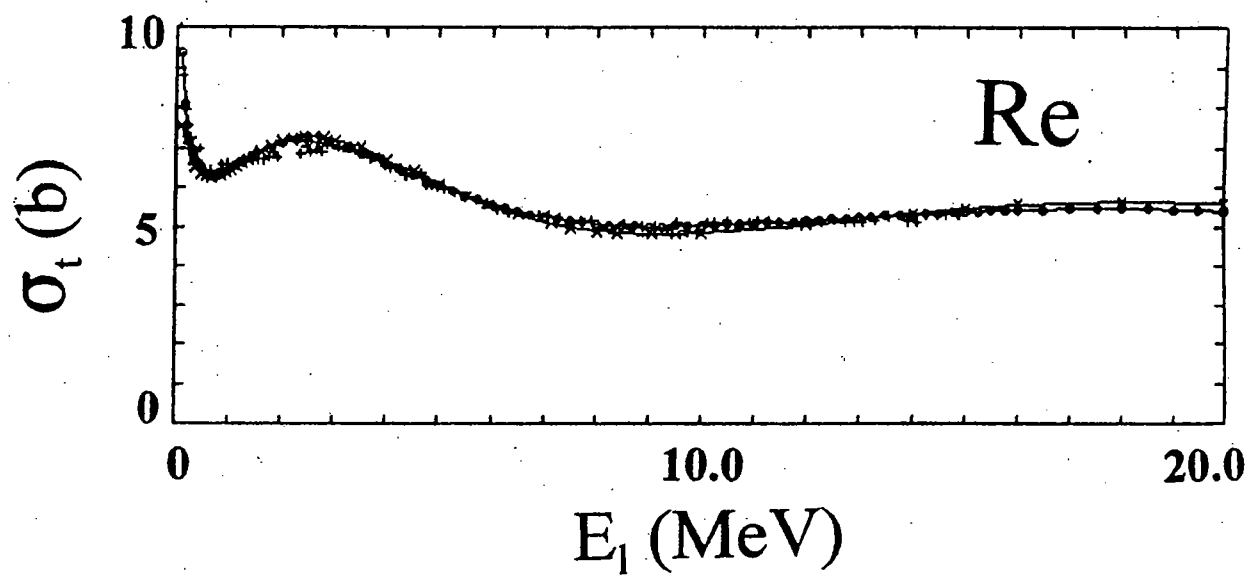


Fig. V-B-2. Upper panel:- Comparison of evaluated and calculated elastic-scattering cross sections of ^{185}Rh . The curve with "x" symbols indicates the results of ROTM calculations, while the curve with "o" symbols denotes the ENDF/B-VI evaluation. The middle panel is the same as the upper panel, but referenced to the ^{187}Re isotope. The lower panel compares the experimental results (symbols) for the inelastic excitation of the first excited level of the g.s. rotational band with the elemental results implied by the ENDF/B-VI isotopic files (curve).

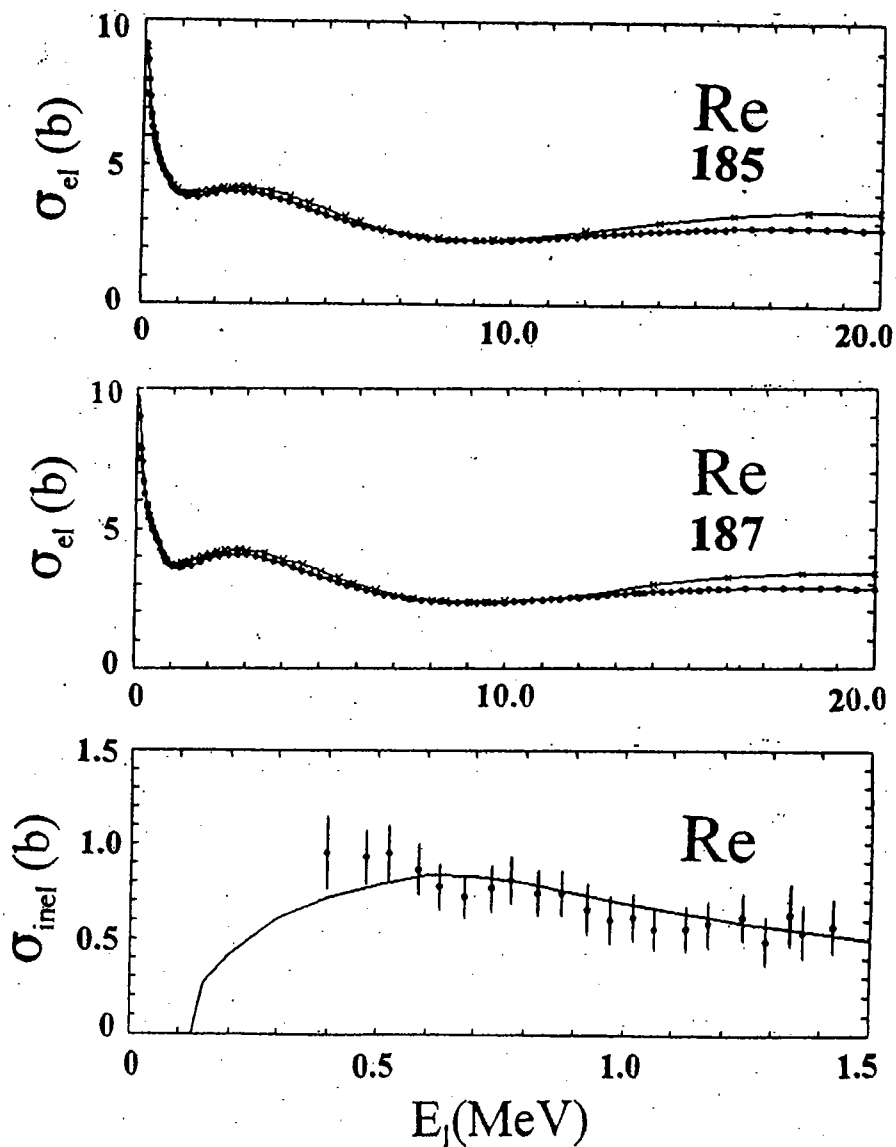


Fig. A-1. The elemental rhenium total cross section data base (symbols) and the END/B-VI evaluation (curve).

